Results in Physics 35 (2022) 105292

Contents lists available at ScienceDirect

Results in Physics

journal homepage: www.elsevier.com/locate/rinp

A novel fractal-fractional order model for the understanding of an oscillatory and complex behavior of human liver with non-singular kernel

Saima Rashid [a,*], Fahd Jarad [b,c,d,*], Abdulaziz Garba Ahmad [e]

[a] Department of Mathematics, Government College University, Faisalabad 38000, Pakistan
[b] Department of Mathematics, Cankaya University, Ankara, Turkey
[c] Department of Mathematics, King Abdulaziz University, Jeddah, Saudi Arabia
[d] Department of Medical Research, China Medical University Hospital, China Medical University, Taichung, Taiwan
[e] Department of Mathematics Programme, National Mathematical Centre Abuja, Nigeria

ARTICLE INFO

MSC:
26A51
26A33
26D07
26D10
26D15

Keywords:
Fractional human liver model
Atangana–Baleanu fractional derivative operator
Fractal-fractional derivative operator
Modified Adams–Bashforth method
Newton polynomial approach

ABSTRACT

Scientists and researchers are increasingly interested in numerical simulations of infections with non-integer orders. It is self-evident that conventional epidemiological systems can be given in a predetermined order, but fractional-order derivative systems are not stable orders. The fractional derivative proves increasingly effective in representing real-world issues when it has a non-fixed order. Various novel fractional operator notions, including special functions in the kernel, have been presented in recent decades, which transcend the constraints of prior fractional order derivatives. These novel operators have been shown to be useful in simulating scientific and technical challenges. The fractal-fractional operator is a relatively modern fractional calculus operator that has been proposed. Besides that, we propose a new technique and implement it in a human liver model and want to investigate its dynamics. In the context of this novel operator, we demonstrate certain interesting findings for the human liver model. The findings of the uniqueness and existence will be revealed. We describe modeling estimates for the proposed model using an innovative numerical method that has never been used before for a human liver model of this type. Additionally, graphical illustrations are demonstrated for both fractal and fractional orders. It is expected that the fractal-fractional approach is more invigorating and effective for epidemic models than the fractional operator.

Introduction

The liver is an important component in the living organism's system that serves as a major facilitator for a variety of homeostasis functions. It modulates plasma circulation, blood coagulation factors, and thrombosis, maintains our immunity mechanism, disintegrates several of the pharmaceuticals we consume, and exfoliates numerous hazardous chemicals in our bodies, such as alcoholism. The primary function of the liver is to maintain enzyme osmotic equilibrium in multiple metabolic mechanisms such as oxidative metabolism, proteolysis, phosphorylation, and aerobic respiration [1].

Hepatitis disorders include infectious diseases such as hepatitis B virus and hepatitis C virus infections, as well as malignant ailments such as renal cell carcinoma and liver cirrhosis, and hyperlipidemia [2].

A variety of medical procedures and therapeutic investigative examinations, such as liver CT and MRI, are available. Plasma levels of hemoglobin, alanine aminotransferase, cysteine performance improvements, alkaline phosphatase, spectral hydroxylase, 50 nucleotidase, apolipoprotein, and a-fetoprotein are among the many standardized experimental hepatic examinations being used regularly to appraise liver capability and as procedure follow-up for liver inhibition caregivers. The identification of liver metabolic indicators would help the practitioner make the best therapeutic recommendations for their patients [3].

Bromsulphthalein (BSP) is an electrophilic phthalein pigment that is extensively utilized in the monitoring of liver cirrhosis. Rosenthal and White [4] demonstrated in 1925 that systemically inserted BSP is eliminated by the liver, implying that this would be a responsive indication of liver functionality, with hepatic failure delaying BSP clearance from the plasma. There seem to be a variety of factors that contribute to BSP accumulation, including proper circulation supply to the liver, appropriate liver enzyme activities, and regular bile evacuation. As a result of the deterioration in causes, there is an increase in BSP levels in the bloodstream [5,6]. The BSP diagnostic is simple to perform: the individual should be starving after receiving a 5 mg/kg BSP intramuscular transfusion, then extract 5 to 10 ml of plasma

* Corresponding authors.
E-mail addresses: saimarashid@gcuf.edu.pk (S. Rashid), fahd@cankaya.edu.tr (F. Jarad), agarbaahmad@yahoo.com (A.G. Ahmad).

https://doi.org/10.1016/j.rinp.2022.105292
Received 10 December 2021; Received in revised form 19 January 2022; Accepted 29 January 2022
Available online 11 February 2022

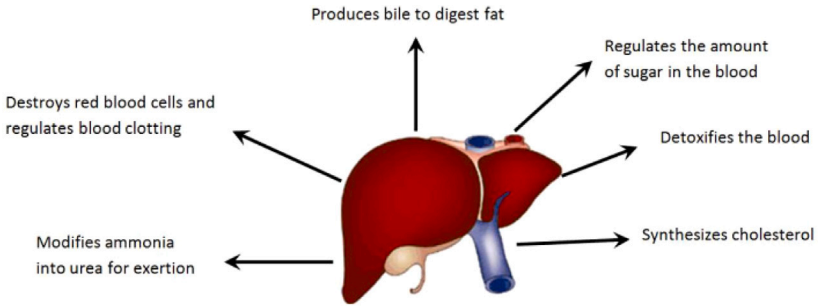

Fig. 1. Liver.

between 25 and 45 min after the inoculation and enable the samples to coagulate. After that, segregate the plasma and determine how much dye is in each individual specimen. This screening is characterized by non-chemicals that are generated predominantly through biliary at a ratio of 10 percent to 15 percent per minute (see Fig. 1).

Fractional calculus (FC) has been frequently employed for biomedical processes; see [7–12]. It has been demonstrated that implementing a fractional method to represent the mechanism is far superior to adopting an integer order optimization since it has the analysis to help understand the actual evidence and several significant qualities. Aside from that, its recollection and inheritance features enable it to be extremely valuable in simulating and interpreting real phenomena. Numerous notions or expressions in fractional calculus are beneficial for modeling infection transmission, including the Atangana–Baleanu, Caputo–Fabrizio, and Caputo derivatives [13–15]. The aforementioned two are more essential, and each one, in particular, is preferable to the previous since it has a generalized Mittag-Leffler function as a non-singular/non-local kernel, as well as the benefit of being able to represent sickness characteristics adequately. Several formulations for modeling techniques have proven to be useful in the literature, see [16–18]. Certain fractional operators can be deployed independently or in tandem to represent contagious disorders. Additional papers relating to fractional derivatives and their applications to a spectrum of challenges can indeed be found in [19–25]. The researchers investigated fractional derivatives and implemented them with serious challenges, then published their findings. For example, Gómez et al. [26] investigates circuit modeling in fractional derivatives. Singh et al. [27] derived the transport equation occurring in fractal porous media by an efficient computational method, Veeresha et al. [28] contemplated the fractional Klein–Gordon–Schrödinger equations via a nonsingular kernel, Baleanu et al. [29] expounded a fractional model and optimal control of a tumor-immune surveillance with a nonsingular derivative operator and many more.

Atangana et al. [30] proposed an innovative conception of non-local formulations for FDEs called the fractal-fractional operator (FFO), which incorporates both fractal and fractional techniques. In several scientific disciplines, especially epidemiology, the aforesaid operators have been used as effective computational methods to produce increasingly intriguing findings. Wang and Khan [31] presented the numerical simulation of a fractional model of bank data with fractal-fractional Atangana–Baleanu derivative technique. Li et al. [32] examined the fractional bank data with a fractal-fractional Caputo derivative. Ghanbari and Gomez [8] used fractal-fractional derivatives in the sense of Caputo and AB-fractional derivatives to analyze two avian influenza epidemic models.

Inspired by the work of Ameen et al. [33] and Baleanu et al. [34], the aim of this research is to analyze the human liver model via the new Atangana–Baleanu FF operator. We integrate this revolutionary idea to the human liver model and explore at a certain innovative liver dynamics. Based to the researchers' perspective, no one has extended the notion of fractal-fractional operator to liver complexities earlier, consequently this is an unique approach. For physicians and academics engaged on modeling techniques, the incorporation of asymptomatic individuals and their assessment in fractal-fractional derivative will serve as a stepping stone of exploration. In Section "Preliminaries", we go through the core concepts of fractalfractional calculus. Sections 3 describe the equilibrium stability of the problem and methods to generate and the results in the classical and fractional cases are demonstrated in Section "Configuration and analysis of the fractional order model". Section "Existence and uniqueness results" discusses fractional frameworks and their numerical findings, as well as their prevalence and novelty using a comprehensive mathematical technique. Section "The fractal-fractional human liver model" implements the Mittag-Leffler functionalities approach alongside the fractal-fractional (FF) operator in the framework. Also, the algorithm for performing simulations of fractional modeling and the FF model is simply presented. The simulating findings for fractional and fractal-fractional models are investigated in various parts of this section, whereas the projected findings have been summarized in Section " Numerical configuration of fractional human liver model".

Preliminaries

Before proceeding on to the mathematical description, it really is essential to review certain basic FF operator concepts. Take into account the mapping $\mathbf{x}(\mathbf{t})$, that is continuous and fractal differentiable over the interval $[c, d]$ having fractal dimension $\mathfrak{p}$ and fractional order α, and the descriptions presented in [30].

Definition 1 ([30]). We say that the FFO of $\mathbf{x}(\mathbf{t})$ having power law kernel in terms of Riemann–Liouville (RL) can be described as follows:

$$^{FFP}\mathbf{D}_{0,\mathbf{t}}^{\alpha,\mathfrak{p}}(\mathbf{x}(\mathbf{t})) = \frac{1}{\Gamma(\mathbf{r}-\alpha)}\frac{d}{d\mathbf{t}^{\mathfrak{p}}}\int_0^{\mathbf{t}}(\mathbf{t}-\mathbf{s})^{\mathbf{r}-\alpha-1}\mathbf{x}(\mathbf{s})d\mathbf{s}, \tag{1}$$

where $\frac{d\mathbf{x}(\mathbf{s})}{d\mathbf{s}^{\mathfrak{p}}} = \lim_{\mathbf{t}\mapsto\mathbf{s}}\frac{\mathbf{x}(\mathbf{t})-\mathbf{x}(\mathbf{s})}{\mathbf{t}^{\mathfrak{p}}-\mathbf{s}^{\mathfrak{p}}}$ and $\mathbf{r}-1<\alpha, \mathfrak{p}\le\mathbf{r}\in\mathbb{N}$.

Definition 2 ([30]). We say that the FFO of $\mathbf{x}(\mathbf{t})$ having exponential kernel in terms of RL can be described as follows:

$$^{FFE}\mathbf{D}_{0,\mathbf{t}}^{\alpha,\mathfrak{p}}(\mathbf{x}(\mathbf{t})) = \frac{\mathbf{q}(\alpha)}{1-\alpha}\frac{d}{d\mathbf{t}^{\mathfrak{p}}}\int_0^{\mathbf{t}}\exp\Big(-\frac{\alpha}{1-\alpha}(\mathbf{t}-\mathbf{s})\Big)\mathbf{x}(\mathbf{s})d\mathbf{s}, \tag{2}$$

such that $\mathbf{q}(0)=\mathbf{q}(1)=1$ having $\alpha>0,\ \mathfrak{p}\le\mathbf{r}\in\mathbb{N}$.

Definition 3 ([30]). We say that the FFO of $\mathbf{x}(\mathbf{t})$ having Mittag-Leffler kernel in terms of RL can be described as follows:

$$^{FFM}\mathbf{D}_{0,\mathbf{t}}^{\alpha,\mathfrak{p}}(\mathbf{x}(\mathbf{t})) = \frac{\mathbb{AB}(\alpha)}{1-\alpha}\frac{d}{d\mathbf{t}^{\mathfrak{p}}}\int_0^{\mathbf{t}}E_{\alpha}\Big(-\frac{\alpha}{1-\alpha}(\mathbf{t}-\mathbf{s})\Big)\mathbf{x}(\mathbf{s})d\mathbf{s}, \tag{3}$$

such that $\mathbb{AB}(\alpha)=1-\alpha+\frac{\alpha}{\Gamma(\alpha)}$ having $\alpha>0,\ \mathfrak{p}\le 1\in\mathbb{N}$.

Definition 4 ([30]). The respective FF integral version of (1) is stated as follows:

$$^{FFP}\mathbb{J}_{0,\mathbf{t}}^{\alpha}(\mathbf{x}(\mathbf{t})) = \frac{\mathfrak{p}}{\Gamma(\alpha)}\int_0^{\mathbf{t}}(\mathbf{t}-\mathbf{s})^{\alpha-1}\mathbf{s}^{\mathfrak{p}-1}\mathbf{x}(\mathbf{s})d\mathbf{s}. \tag{4}$$

Definition 5 ([30]). The respective FF integral version of (2) is stated as follows:

$$^{FFE}\mathbb{J}^{\alpha}_{0,\mathbf{t}}(\mathbf{x}(\mathbf{t})) = \frac{\alpha \mathfrak{p}}{\mathbf{q}(\alpha)} \int_0^{\mathbf{t}} \mathbf{s}^{\mathfrak{p}-1}\mathbf{x}(\mathbf{s})d\mathbf{s} + \frac{\mathfrak{p}(1-\alpha)\mathbf{t}^{\mathfrak{p}-1}\mathbf{x}(\mathbf{t})}{\mathbf{q}(\alpha)}. \tag{5}$$

Definition 6 ([30]). The respective FF integral version of (3) is stated as follows:

$$^{FFM}\mathbb{J}^{\alpha}_{0,\mathbf{t}}(\mathbf{x}(\mathbf{t})) = \frac{\alpha \mathfrak{p}}{\mathbb{AB}(\alpha)} \int_0^{\mathbf{t}} \mathbf{s}^{\mathfrak{p}-1}(\mathbf{t}-\mathbf{s})^{\alpha-1}\mathbf{x}(\mathbf{s})d\mathbf{s} + \frac{\mathfrak{p}(1-\alpha)\mathbf{t}^{\mathfrak{p}-1}\mathbf{x}(\mathbf{t})}{\mathbb{AB}(\alpha)}. \tag{6}$$

Definition 7 ([14]). Let $\mathbf{x} \in H^1(\delta,\gamma)$, $\delta < \gamma$ and the ABC derivative operator is stated as follows:

$$^{ABC}_{\mathbf{c}}\mathbf{D}^{\alpha}_{\mathbf{t}}(\mathbf{x}(\mathbf{t})) = \frac{\mathbb{AB}(\alpha)}{1-\alpha} \int_{\mathbf{c}}^{\mathbf{t}} \mathbf{x}'(\mathbf{s}) E_{\alpha}\Big(-\frac{\alpha(\mathbf{t}-\mathbf{s})^{\alpha}}{1-\alpha}\Big)d\mathbf{s}, \quad \alpha \in [0,1], \tag{7}$$

where $\mathbb{AB}(\alpha)$ denotes the normalization function.

Description of the model

Čelechovská [35] presented integer-order characteristics of the human liver in 2004. The researcher analyzed the apparent clinical information collected by the Bromsulphthalein (BSP) examination to determine the parameters within this study. Assume that $\mathcal{U}(\mathbf{t})$, $\mathcal{V}(\mathbf{t})$ and $\mathcal{W}(\mathbf{t})$ denote the concentration of BSP in the blood, liver, and bile at time $\mathbf{t}$, respectively. Then there is Čelechovská integer-order model, which is stated in [35]:

$$\begin{aligned}
\frac{d\mathcal{U}(\mathbf{t})}{d\mathbf{t}} &= -\bar{A}\mathcal{U}(\mathbf{t}) + \bar{B}\mathcal{V}(\mathbf{t}),\\
\frac{d\mathcal{V}(\mathbf{t})}{d\mathbf{t}} &= \bar{A}\mathcal{U}(\mathbf{t}) - (\bar{B}+\bar{C})\mathcal{V}(\mathbf{t}),\\
\frac{d\mathcal{W}(\mathbf{t})}{d\mathbf{t}} &= \bar{C}\mathcal{V}(\mathbf{t}),
\end{aligned} \tag{8}$$

supplements with the initial conditions $\mathcal{U}(0) = \mathbb{I}$, $\mathcal{V}(0) = 0, \mathcal{W}(0) = 0$. Also, the transition rates are indicated by the parameters $\bar{A}, \bar{B}, \bar{C}$ and $\bar{D}$.

To improve the framework, we need to exchange the first-order derivatives with new fractional-order ABC derivatives, as shown by

$$\begin{aligned}
^{ABC}\mathbf{D}^{\alpha}_{\mathbf{t}}\mathcal{U}(\mathbf{t}) &= -\bar{A}\mathcal{U}(\mathbf{t}) + \bar{B}\mathcal{V}(\mathbf{t}),\\
^{ABC}\mathbf{D}^{\alpha}_{\mathbf{t}}\mathcal{V}(\mathbf{t}) &= \bar{A}\mathcal{U}(\mathbf{t}) - (\bar{B}+\bar{C})\mathcal{V}(\mathbf{t}),\\
^{ABC}\mathbf{D}^{\alpha}_{\mathbf{t}}\mathcal{W}(\mathbf{t}) &= \bar{C}\mathcal{V}(\mathbf{t}).
\end{aligned} \tag{9}$$

It is worth noting that the right-hand side of the equations in system (9) has the dimension time^{-1}; So when the derivative order is modified, the dimension of the left-hand side becomes time. We changed the parameters as follows to avoid dimensional discrepancy [35]:

$$\begin{aligned}
^{ABC}\mathbf{D}^{\alpha}_{\mathbf{t}}\mathcal{U}(\mathbf{t}) &= -\bar{A}^{\alpha}\mathcal{U}(\mathbf{t}) + \bar{B}^{\alpha}\mathcal{V}(\mathbf{t}),\\
^{ABC}\mathbf{D}^{\alpha}_{\mathbf{t}}\mathcal{V}(\mathbf{t}) &= \bar{A}^{\alpha}\mathcal{U}(\mathbf{t}) - (\bar{B}^{\alpha}+\bar{C}^{\alpha})\mathcal{V}(\mathbf{t}),\\
^{ABC}\mathbf{D}^{\alpha}_{\mathbf{t}}\mathcal{W}(\mathbf{t}) &= \bar{C}^{\alpha}\mathcal{V}(\mathbf{t}).
\end{aligned} \tag{10}$$

As for clarity, suppose that $\mathbf{a} = \bar{A}^{\alpha}$, $b_1 = \bar{B}^{\alpha}$, $\mathbf{c} = \bar{C}^{\alpha}$, we obtain the fractional model of the human liver as follows:

$$\begin{aligned}
^{ABC}\mathbf{D}^{\alpha}_{\mathbf{t}}\mathcal{U}(\mathbf{t}) &= -\mathbf{a}\mathcal{U}(\mathbf{t}) + \mathbf{b}\mathcal{V}(\mathbf{t}),\\
^{ABC}\mathbf{D}^{\alpha}_{\mathbf{t}}\mathcal{V}(\mathbf{t}) &= \mathbf{a}\mathcal{U}(\mathbf{t}) - (\mathbf{b}+\mathbf{c})\mathcal{V}(\mathbf{t}),\\
^{ABC}\mathbf{D}^{\alpha}_{\mathbf{t}}\mathcal{W}(\mathbf{t}) &= \mathbf{c}\mathcal{V}(\mathbf{t}).
\end{aligned} \tag{11}$$

Configuration and analysis of the fractional order model

In this section, we will look at several of the fractional order model's features. We proceed with the fractional order model (10) affirmation. Regarding the model (10), we explain the stability of the EP before demonstrating that the fractional order model solution is invariably positive when the initial values and parameters are positive.

Certainly, the reinforcement of the framework of the BSP experiment can be perceived diagnostically by the actual amount of BSP transfused into the plasma at once as a "intravenous dose". This confirmation can be demonstrated quantitatively by including formulae in the fractional order model. Then, we have

$$^{ABC}_{0}\mathbf{D}^{\alpha}_{\mathbf{t}}\mathcal{U}(\mathbf{t}) + {}^{ABC}_{0}\mathbf{D}^{\alpha}_{\mathbf{t}}\mathcal{V}(\mathbf{t}) + {}^{ABC}_{0}\mathbf{D}^{\alpha}_{\mathbf{t}}\mathcal{W}(\mathbf{t}) = 0 \tag{12}$$

In view of the linearity property of the ABC fractional derivative, we can represent (12) as follows:

$$^{ABC}_{0}\mathbf{D}^{\alpha}_{\mathbf{t}}\big[\mathcal{U}(\mathbf{t}) + \mathcal{V}(\mathbf{t}) + \mathcal{W}(\mathbf{t})\big] = 0, \tag{13}$$

the above expression is stated as

$$\mathcal{U}(\mathbf{t}) + \mathcal{V}(\mathbf{t}) + \mathcal{W}(\mathbf{t}) = Constant > 0, \quad \forall \mathbf{t} > 0. \tag{14}$$

This indicates that the entire amount of BSP remains constant, which is totally compatible with the medical clarification given above.

Equilibrium and stability

To investigate the stability of the ABC fractional order system, (11). It is extremely important to analyze the smaller dimensional system. Then, we have

$$^{ABC}\mathbf{D}^{\alpha}_{\mathbf{t}}\mathcal{U} = 0, \quad {}^{ABC}\mathbf{D}^{\alpha}_{\mathbf{t}}\mathcal{V} = 0. \tag{15}$$

For resolving (15), then the ABC fractional liver model (10) has a unique equilibrium at $\mathcal{E} = (0,0)$. Therefore, the parameters $\bar{A}^{\alpha}_1, \bar{B}^{\alpha}_1, \bar{C}^{\alpha}_1 > 0$. As contrast to the feasible domain of the particular set of conditions, the fractional-order system has the largest equilibrium region (see, [36]). We are now able to declare and demonstrate the equilibrium problem and its basic stability results.

Theorem 1. *The equilibrium Ξ of the fractional order model (10) is locally asymptotically stable if $\bar{A}^{\alpha} + \bar{B}^{\alpha} + \bar{C}^{\alpha} \geq 4\bar{A}^{\alpha}\bar{C}^{\alpha}$, otherwise it is unstable.*

Proof. The matrix of the fractional order system (10) is

$$\mathbb{Q} = \begin{bmatrix} -\bar{A}^{\alpha} & \bar{B}^{\alpha} \\ \bar{A}^{\alpha} & -(\bar{B}^{\alpha}+\bar{C}^{\alpha}) \end{bmatrix}, \tag{16}$$

and the characteristic values of this matrix, given by the algebraic equation

$$det(\mathbb{Q} - \lambda\mathcal{E}) = \lambda^2 + (\bar{A}^{\alpha} + \bar{B}^{\alpha} + \bar{C}^{\alpha}) + \bar{A}^{\alpha}\bar{C}^{\alpha} = 0,$$

are

$$\lambda_{1,2} = \frac{-(\bar{A}^{\alpha} + \bar{B}^{\alpha} + \bar{C}^{\alpha}) \pm \sqrt{(\bar{A}^{\alpha} + \bar{B}^{\alpha} + \bar{C}^{\alpha})^2 - 4\bar{A}^{\alpha}\bar{C}^{\alpha}}}{2}.$$

If $\bar{A}^{\alpha}$, $\bar{B}^{\alpha}$, and $\bar{C}^{\alpha}$ are positive, then

$$(\bar{A}^{\alpha} + \bar{B}^{\alpha} + \bar{C}^{\alpha})^2 - 4\bar{A}^{\alpha}\bar{C}^{\alpha} \geq 0.$$

So the characteristic values $\lambda_{1,2}$ are negative, which means that the solution $\mathcal{U}(\mathbf{t}) = 0$, $\mathcal{V}(\mathbf{t}) = 0$ corresponding to the equilibrium $\mathcal{E}$ of (10) is globally asymptotically stable. □

Now we state the epidemiologically feasible (non-negative and boundedness) region of this investigation in Theorem 2 and demonstrate that the region is positively invariant and bounded.

Theorem 2. *The epidemiologically feasible region of human liver model (10) is given by*

$$\Phi =: \big\{(\mathcal{U},\mathcal{V},\mathcal{W}) \in \mathbb{R}^3_+ : 0 \leq \mathcal{U} + \mathcal{V} + \mathcal{W} = \mathcal{N}\big\}. \tag{17}$$

The existence and uniqueness of the solution of model (10) are now proved, and it remains to show that the set Φ defined in (17) is positively invariant. The following lemma will be used for the proof of Theorem 2.

Lemma 3 ([37]). *Suppose* $\mathcal{G}(\mathbf{x}) \in \mathbb{C}[\mathbf{a},\mathbf{b}]$ *and let* ${}_{0}^{ABC}\mathbf{D}_{\mathbf{t}}^{\alpha}\mathcal{G}(\mathbf{x}) \in \mathbb{C}[\mathbf{a},\mathbf{b}]$, *when* $\alpha \in (0,1]$. *Then we have* $\mathcal{G}(\mathbf{x}) = \mathcal{G}(\mathbf{a}) + \frac{1}{\Gamma(\alpha)}\,{}_{0}^{ABC}\mathcal{G}(\xi)(\mathbf{x}-\mathbf{a})^{\alpha}$, *when* $0 \le \xi \le \mathbf{x}$.

Theorem 4. *The region* $\Phi_{+} = \{(\mathcal{U},\mathcal{V},\mathcal{W}); \mathcal{U} > 0, \mathcal{V} \ge 0, \mathcal{W} \ge 0\}$ *is a positive invariant set for the system* (10).

Proof. By means of the fractional order system (10), we conclude that

$$\begin{aligned}
&{}^{ABC}\mathbf{D}_{\mathbf{t}}^{\alpha}\Big|_{\mathcal{U}=0} = \bar{B}^{\alpha}\mathcal{V}(\mathbf{t}) \ge 0,\\
&{}^{ABC}\mathbf{D}_{\mathbf{t}}^{\alpha}\Big|_{\mathcal{V}=0} = \bar{A}^{\alpha}\mathcal{U}(\mathbf{t}) \ge 0,\\
&{}^{ABC}\mathbf{D}_{\mathbf{t}}^{\alpha}\Big|_{\mathcal{W}=0} = \bar{C}^{\alpha}\mathcal{V}(\mathbf{t}) \ge 0.
\end{aligned} \tag{18}$$

From (18) and Lemma 3, the requisite objective is validated i.e., the solution will remain in Φ and therefore this region for the fractional order system (10) is a positive invariant set. □

Another distinguishing feature of the preferred scheme is its boundedness. As a result, it is worthwhile to demonstrate that the solution of the fractional order system (10) is bounded, as stated in the following theorem.

Theorem 5. *The region* $\Phi = \{(\mathcal{U},\mathcal{V},\mathcal{W}) \in \mathbb{R}_{+}^{3} : 0 \le \mathcal{U}+\mathcal{V}+\mathcal{W} = \mathcal{N}\}$ *is a positive invariant set for the fractional order system* (10).

Proof. To establish the boundedness of the solution of fractional order model (10), taking into consideration that all parameters are positive, the explicit solutions of the system (10) are presented by

$$\begin{aligned}
U(\mathbf{t}) &= \frac{(\bar{A}^{\alpha}-\bar{B}^{\alpha}-\bar{C}^{\alpha})\big[E_{\alpha}(\lambda_2\mathbf{t}^{\alpha}) - E_{\alpha}(\lambda_1\mathbf{t}^{\alpha})\big]\mathbb{I}}{2\sqrt{(\bar{A}^{\alpha}+\bar{B}^{\alpha}+\bar{C}^{\alpha})^2 - 4\bar{A}^{\alpha}\bar{C}^{\alpha}}}\\
&\quad + \frac{\mathbb{I}}{2}\big[E_{\alpha}(\lambda_2\mathbf{t}^{\alpha}) + E_{\alpha}(\lambda_1\mathbf{t}^{\alpha})\big] > 0,\\
\mathcal{V}(\mathbf{t}) &= \frac{-\bar{A}^{\alpha}\big[E_{\alpha}(\lambda_2\mathbf{t}^{\alpha}) - E_{\alpha}(\lambda_1\mathbf{t}^{\alpha})\big]\mathbb{I}}{2\sqrt{(\bar{A}^{\alpha}+\bar{B}^{\alpha}+\bar{C}^{\alpha})^2 - 4\bar{A}^{\alpha}\bar{C}^{\alpha}}}\mathbf{t}^{1-\alpha} \ge 0,
\end{aligned} \tag{19}$$

where λ_1 and λ_2 are the eigenvalues of $\mathbb{Q}$. Now, implementing Laplace transform for the third compartment of (10) supplemented with the initial conditions, then we have

$$\mathbf{W}(s) = \mathbf{H}(s)\mathbf{V}(s),$$

therefore

$$\mathbf{H}(s) = \frac{\bar{C}^{\alpha}}{s^{\alpha}}, \tag{20}$$

that can be written as $\mathcal{W}(\mathbf{t}) = \mathcal{H}(\mathbf{t}) * \mathcal{V}(\mathbf{t})$, this shows that $\mathcal{W}(\mathbf{t})$ is the Laplace convolution of the two mappings $\mathcal{H}(\mathbf{t})$ and $\mathcal{V}(\mathbf{t})$. Following the work [38] and implementing the inverse Laplace transform, the solution is presented by

$$\mathcal{N}(\mathbf{t}) = \bar{C}^{\alpha} - \bar{C}^{\alpha}\frac{d}{d\mathbf{t}}\int_{0}^{\mathbf{t}} E_{\alpha}\Big(\bar{C}^{\alpha}(\mathbf{t}-\mathbf{x})^{\alpha}d\mathbf{x}\Big) + \mathcal{N}(0)E_{\alpha}(\bar{C}^{\alpha}\mathbf{t}^{\alpha}), \tag{21}$$

where $E_{\alpha,\beta}$ indicates the Mittag-Leffler function. Utilizing the fact that the Mittag-Leffler function has asymptotic behavior

$$E_{\alpha,\beta}(z) \approx \sum_{\mathcal{K}=1}^{q} z^{-\mathcal{K}}/\Gamma(\beta-\alpha\mathcal{K}) + \mathcal{O}(|z|^{-1-q}), \quad |z| \mapsto \infty, \quad \frac{\alpha\pi}{2} < |Arg(z)| \le \pi,$$

it is not difficult to observe that $\mathcal{N}(\mathbf{t}) \mapsto \bar{C}^{\alpha}$ as $\mathbf{t} \mapsto \infty$. Hence (17) is the biologically feasible region of the system (10). □

Existence and uniqueness results

We investigate the existence of a unique solution for the system (11) using fixed point theory. To use it, we immediately transform the liver model (11) into an integral equation incorporating the fractional order integral operator (7). We can write the system (11) as follows:

$$\begin{cases}
{}^{ABC}\mathbf{D}_{\mathbf{t}}^{\alpha}\Omega(\mathbf{t}) = \Lambda(\mathbf{t},\Omega(\mathbf{t})),\\
\Omega(0) = \Omega_0, \quad 0 < \mathbf{t} < \mathbf{T} < \infty.
\end{cases} \tag{22}$$

The vector $\Omega(\mathbf{t}) = (\mathcal{U},\mathcal{V},\mathcal{W})$ represents the state of variables while $\Omega_0 = \big(\mathcal{U}(0),\mathcal{V}(0),\mathcal{W}(0)\big)$ presents the corresponding initial conditions defined in (22). Furthermore, a continuous vector mapping is signifies by Λ as follows:

$$\Lambda = \begin{bmatrix}\Lambda_1\\ \Lambda_2\\ \Lambda_3\end{bmatrix} = \begin{bmatrix}-\mathbf{a}\mathcal{U}+\mathbf{b}\mathcal{V}\\ \mathbf{a}\mathcal{U}-(\mathbf{b}+\mathbf{c})\mathcal{V}\\ \mathbf{c}\mathcal{V}\end{bmatrix}.$$

Also, the mapping Λ fulfills the Lipschitz assumption described as:

$$\Big\|\Lambda(\mathbf{t},\Omega_1(\mathbf{t})) - \Lambda(\mathbf{t},\Omega_2(\mathbf{t}))\Big\| \le \mathbb{L}_{\omega}\Big\|\Omega_1(\mathbf{t}) - \Omega_2(\mathbf{t})\Big\|, \quad \mathbb{L}_{\omega} > 0. \tag{23}$$

To achieve the requisite outcome, we prove the accompanying theorem.

Theorem 6. *For the model* (22) *there exists a unique solution if*

$$\frac{1-\alpha}{\mathcal{AB}(\alpha)}\mathbb{L}_{\Omega} + \frac{\alpha}{\mathcal{AB}(\alpha)\Gamma(\alpha)}\mathbf{T}_{\max}^{\alpha}\mathbb{L}_{\Omega} < 1. \tag{24}$$

Proof. Employing Definition 7 to the Problem (22), then the system reduces to Volterra integral equation as follows:

$$\Omega(\mathbf{t}) = \Omega_0 + \frac{1-\alpha}{\mathbb{AB}(\alpha)}\Lambda(\mathbf{t},\Omega(\mathbf{t})) + \frac{\alpha}{\mathbb{AB}(\alpha)\Gamma(\alpha)}\int_{0}^{\mathbf{t}}(\mathbf{t}-\tau)^{\alpha-1}\Lambda(\tau,\Omega(\tau))d\tau. \tag{25}$$

Suppose that $\mathcal{T} = (0,\mathbf{T})$ and the operator $\mathbf{F} : \mathbb{C}(\mathcal{T},\mathbb{R}^3) \mapsto \mathbb{C}(\mathcal{T},\mathbb{R}^3)$ described as

$$\Omega(\mathbf{t}) = \Omega_0 + \frac{1-\alpha}{\mathbb{AB}(\alpha)}\Lambda(\mathbf{t},\Omega(\mathbf{t})) + \frac{\alpha}{\mathbb{AB}(\alpha)\Gamma(\alpha)}\int_{0}^{\mathbf{t}}(\mathbf{t}-\tau)^{\alpha-1}\Lambda(\tau,\Omega(\tau))d\tau. \tag{26}$$

As a result, (25) reduces to the following form:

$$\Omega(\mathbf{t}) = \mathbf{F}\big[\Omega(\mathbf{t})\big]. \tag{27}$$

Assume that the supremum norm on $\mathcal{T}$ denoted by $\|.\|_{\mathcal{T}}$ and represented as:

$$\Big\|\Omega(\mathbf{t})\Big\|_{\mathcal{T}} = \sup_{\mathbf{t}\in\mathcal{T}}\Big\|\Omega(\mathbf{t})\Big\|, \quad \Omega(\mathbf{t}) \in \mathbb{C}. \tag{28}$$

It is evident that $\mathbb{C}(\mathcal{T},\mathbb{R}^3)$ having the norm $\|.\|_{\mathcal{T}}$ is a Banach space. In addition, the resulting inequality is simply demonstrated:

$$\Big\|\int_{0}^{\mathbf{t}}\mathcal{K}(\mathbf{t},\tau)\Omega(\tau)d\tau\Big\| \le \mathbf{T}\Big\|\mathcal{K}(\mathbf{t},\tau)\Big\|_{\mathcal{T}}\Big\|\Omega(\mathbf{t})\Big\|_{\mathcal{T}}, \quad \forall\Omega(\mathbf{t}) \in \mathbb{C}(\mathcal{T},\mathbb{R}^{+}),\\ \mathcal{K}(\mathbf{t},\tau) \in \mathbb{C}(\mathcal{T}^2,\mathbb{R}) \tag{29}$$

such that

$$\Big\|\mathcal{K}(\mathbf{t},\tau)\Big\|_{\mathcal{T}} = \sup_{\mathbf{t},\tau\in\mathcal{T}}\Big|\mathcal{K}(\mathbf{t},\tau)\Big|. \tag{30}$$

Applying (27), we can achieve

$$\begin{aligned}
\Big\|\mathbf{F}\big[\Omega_1(\mathbf{t})\big] - \mathbf{F}\big[\Omega_2(\mathbf{t})\big]\Big\|_{\mathcal{T}} \le{}& \Big\|\frac{1-\alpha}{\mathbb{AB}(\alpha)}\Big(\Lambda(\mathbf{t},\Omega_1(\mathbf{t})) - \Lambda(\mathbf{t},\Omega_2(\mathbf{t}))\Big)\\
&+ \frac{\alpha}{\mathbb{AB}(\alpha)\Gamma(\alpha)}\int_{0}^{\mathbf{t}}(\mathbf{t}-\tau)^{\alpha-1}\\
&\times\Big(\Lambda(\tau,\Omega_1(\tau)) - \Lambda(\tau,\Omega_2(\tau))\Big)\Big\|_{\mathcal{T}}.
\end{aligned} \tag{31}$$

Furthermore, combining (23), (29), and triangular inequality, (31) yields:

$$\Big\|\mathbf{F}\big[\Omega_1(\mathbf{t})\big] - \mathbf{F}\big[\Omega_2(\mathbf{t})\big]\Big\|_{\mathcal{T}} \le \Big(\frac{1-\alpha}{\mathbb{AB}(\alpha)}\mathbb{L}_{\Omega} + \frac{\alpha\mathbf{T}_{\max}^{\alpha}}{\mathbb{AB}(\alpha)\Gamma(\alpha)}\mathbb{L}_{\Omega}\Big)\Big\|\Omega_1(\mathbf{t}) - \Omega_2(\mathbf{t})\Big\|_{\mathcal{T}}.$$

Ultimately, we arrive at the following conclusion:

$$\Big\|\mathbf{F}\big[\Omega_1(\mathbf{t})\big] - \mathbf{F}\big[\Omega_2(\mathbf{t})\big]\Big\|_{\mathcal{T}} \le \Upsilon\Big\|\Omega_1(\mathbf{t}) - \Omega_2(\mathbf{t})\Big\|_{\mathcal{T}},$$

where

$$\Upsilon = \frac{1-\alpha}{\mathbb{AB}(\alpha)}\mathbb{L}_{\Omega} + \frac{\alpha\mathbf{T}_{\max}^{\alpha}}{\mathbb{AB}(\alpha)\Gamma(\alpha)}\mathbb{L}_{\Omega}.$$

Since the operator $\mathbf{F}$ satisfies the requirement in (24), that can be a contraction mapping. As a consequence, the system proposed by (22) has a unique solution. □

The fractal-fractional human liver model

In this part, we employ the new fractal-fractional operator to reconstitute the classical integer-order human liver model, utilizing a nonsingular and nonlocal kernel (8). The human liver model that emerges from considering the fractal-fractional operator can be expressed in the subsequent form:

$$\begin{aligned} {}^{FF}\mathbf{D}_{0,\mathbf{t}}^{\alpha,\mathfrak{p}}\left(\mathcal{U}(\mathbf{t})\right) &= -\mathbf{a}\mathcal{U}(\mathbf{t}) + \mathbf{b}\mathcal{V}(\mathbf{t}),\\ {}^{FF}\mathbf{D}_{0,\mathbf{t}}^{\alpha,\mathfrak{p}}\left(\mathcal{V}(\mathbf{t})\right) &= \mathbf{a}\mathcal{U}(\mathbf{t}) - (\mathbf{b}+\mathbf{c})\mathcal{V}(\mathbf{t}),\\ {}^{FF}\mathbf{D}_{0,\mathbf{t}}^{\alpha,\mathfrak{p}}\left(\mathcal{W}(\mathbf{t})\right) &= \mathbf{c}\mathcal{V}(\mathbf{t}), \end{aligned} \tag{32}$$

where ${}^{FF}\mathbf{D}_{0,\mathbf{t}}^{\alpha,\mathfrak{p}}(.)$ denotes the fractal-fractional operator in terms of ABC, where α and $\mathfrak{p}$ symbolize the fractional and fractal orders, respectively.

Existence and uniqueness results of fractal-fractional human liver model

In (32), the existence and uniqueness of the human liver model constructed in the fractal-fractional operator are briefly explained.To do so, we shall develop the general Cauchy problem with a fractal-fractional derivative as follows:

$$\begin{cases} {}^{FF}\mathbf{D}_{0,\mathbf{t}}^{\alpha,\mathfrak{p}}\Theta(\mathbf{t}) = \Xi(\mathbf{t},\Theta(\mathbf{t})),\\ \Theta(0) = \Theta_0. \end{cases} \tag{33}$$

According to Definition 3, the right hand side of (33) provides the following:

$$\frac{\mathbb{AB}(\alpha)}{1-\alpha}\frac{d}{d\mathbf{t}}\int_0^{\mathbf{t}}\Xi(\mathbf{s},\Theta(\mathbf{s}))\bar{E}_{\alpha}\Big(-\frac{\alpha}{1-\alpha}(\mathbf{t}-\mathbf{s})^{\alpha}\Big)d\mathbf{s} = \mathfrak{p}\mathbf{t}^{\mathfrak{p}-1}\Xi(\mathbf{t},\Theta(\mathbf{t})). \tag{34}$$

Continuing to follow the use of the relevant integral, the following results:

$$\Theta(\mathbf{t}) = \frac{1-\alpha}{\mathbb{AB}(\alpha)}\mathfrak{p}\mathbf{t}^{\mathfrak{p}-1}\Xi(\mathbf{t},\Theta(\mathbf{t})) + \frac{\mathfrak{p}\alpha}{\mathbb{AB}(\alpha)\Gamma(\alpha)} \times\int_0^{\mathbf{t}}(\mathbf{t}-\mathbf{s})^{\alpha-1}\Xi(\mathbf{s},\Theta(\mathbf{s}))\mathbf{s}^{\mathfrak{p}-1}d\mathbf{s} + \Theta(0).$$

Applying the Picard–Lindelof technique, we have

$$\prod_{\eta_1}^{\eta_2} = \mathcal{I}_{\mathbf{r}}(\mathbf{t}_{\mathbf{r}}) \times \overline{\mathcal{A}_0(\Theta_0)},$$

where $\overline{\mathcal{I}_{\mathbf{r}}(\mathbf{t}_{\mathbf{r}})} = \left[\mathbf{t}_{\mathbf{r}-\mu_1}, \mathbf{t}_{\mathbf{r}+\mu_1}\right]$, $\overline{\mathcal{A}_0(\Theta_0)} = \left[\mathbf{t}_0-\nu_1, \mathbf{t}_0+\nu_1\right]$.

Likewise, suppose that

$$\mathfrak{H} = \sup_{\mathbf{t}\in\prod_{\eta_1}^{\eta_2}}\left\|\Xi\right\|.$$

Additionally, the norm is formulated as having:

$$\left\|\chi\right\|_{\infty} = \sup_{\mathbf{t}\in\prod_{\eta_1}^{\eta_2}}\left\|\chi\right\|,$$

and propose the operations

$$\mho\Big[\mathcal{C}\left[\mathcal{I}_{\mathbf{r}}(\mathbf{t}_{\mathbf{r}}),\mathcal{A}_{\mathfrak{b}}(\mathbf{t}_{\mathbf{r}})\right]\Big] \longrightarrow \mathcal{C}\left(\mathcal{I}_{\mathbf{r}}(\mathfrak{b}),\mathcal{A}_{\mathfrak{b}}(\mathbf{t}_{\mathbf{r}})\right),$$

stated by

$$\mho\Xi(\mathbf{t}) = \Xi_0 + \frac{1-\alpha}{\mathbb{AB}(\alpha)}\mathfrak{p}\mathbf{t}^{\mathfrak{p}-1}\Xi(\mathbf{t},\Theta(\mathbf{t})) + \frac{\alpha\mathfrak{p}}{\mathbb{AB}(\alpha)\Gamma(\alpha)}\int_0^{\mathbf{t}}(\mathbf{t}-\mathbf{s})^{\alpha-1}\Xi(\mathbf{s},\Theta(\mathbf{s}))\mathbf{s}^{\mathfrak{p}-1}d\mathbf{s}.$$

The fundamental goal is to demonstrate that the above-mentioned operator translates a completely empty metric space upon itself. Additionally, we want to show that it offers contraction mapping capability. To begin with, we demonstrate that

$$\begin{aligned} &\left\|\mho\Theta(\mathbf{t}) - \Theta_0\right\| \le \mathfrak{b},\\ &\left\|\mho\Theta(\mathbf{t}) - \Theta_0\right\| \le \frac{1-\alpha}{\mathbb{AB}(\alpha)}\mathfrak{p}\mathbf{t}^{\mathfrak{p}-1}\left\|\Xi(\mathbf{t},\Theta(\mathbf{t}))\right\|_{\infty}\\ &\quad+\frac{\alpha\mathfrak{p}}{\mathbb{AB}(\alpha)\Gamma(\alpha)}\int_0^{\mathbf{t}}(\mathbf{t}-\mathbf{s})^{\alpha-1}\left\|\Xi(\mathbf{s},\Theta(\mathbf{s}))\right\|\mathbf{s}^{\mathfrak{p}-1}d\mathbf{s}\\ &\le \frac{1-\alpha}{\mathbb{AB}(\alpha)}\mathfrak{p}\mathbf{t}^{\mathfrak{p}-1}\chi + \frac{\alpha\mathfrak{p}}{\mathbb{AB}(\alpha)\Gamma(\alpha)}\chi\int_0^{\mathbf{t}}(\mathbf{t}-\mathbf{s})^{\alpha-1}\mathbf{s}^{\mathfrak{p}-1}d\mathbf{s}. \end{aligned}$$

Substituting $\mathbf{s} = \mathbf{t}\mathbf{x}$, then yields the following

$$\left\|\mho\Theta(\mathbf{t}) - \Theta_0\right\| \le \frac{1-\alpha}{\mathbb{AB}(\alpha)}\mathfrak{p}\mathbf{t}^{\mathfrak{p}-1}\chi + \frac{\alpha\mathfrak{p}}{\mathbb{AB}(\alpha)\Gamma(\alpha)}\chi\mathbf{t}^{\alpha+\mathfrak{p}-1}B_1(\mathfrak{p},\alpha).$$

Thus,

$$\left\|\mho\Theta(\mathbf{t}) - \Theta_0\right\| \le \mathfrak{b} \mapsto \chi < \frac{\mathfrak{b}B_1(\mathfrak{p},\alpha)}{\frac{1-\alpha}{\mathbb{AB}(\alpha)}\mathfrak{p}\mathbf{t}^{\mathfrak{p}-1} + \frac{\alpha\mathfrak{p}}{\mathbb{AB}(\alpha)\Gamma(\alpha)}\mathbf{t}^{\alpha+\mathfrak{p}-1}}$$

Then, assuming $\Theta_1, \Theta_2 \in \mathcal{C}[\mathcal{I}_{\mathbf{r}}(\mathbf{t}_{\mathbf{r}}), \mathcal{A}_{\mathfrak{b}}(\mathbf{t}_{\mathbf{r}})]$, implement the Banach fixed point theorem to arrive at the corresponding consequence:

$$\left\|\mho\Theta_1 - \mho\Theta_2\right\| \le \mathbb{L}_{\Omega}\left\|\Theta - \Theta_2\right\|_{\infty},$$

where $\mathbb{L}_{\Omega} < 1$.

$$\begin{aligned} \left\|\mho\Theta_1 - \mho\Theta_2\right\| &\le \frac{1-\alpha}{\mathbb{AB}(\alpha)}\mathfrak{p}\mathbf{t}^{\mathfrak{p}-1}\left\|\Xi(\mathbf{t},\Theta_1) - \Xi(\mathbf{t},\Theta_2)\right\|\\ &\quad+\frac{\alpha\mathfrak{p}}{\mathbb{AB}(\alpha)\Gamma(\alpha)}\int_0^{\mathbf{t}}(\mathbf{t}-\mathbf{s})^{\alpha-1}\mathbf{s}^{\mathfrak{p}-1}\left\|\Xi(\mathbf{t},\mathbf{s}_1) - \Xi(\mathbf{t},s_2)\right\|d\mathbf{s}, \end{aligned}$$

Thanks to the contraction of the mapping Ξ, we have

$$\begin{aligned} \left\|\mho\Theta_1 - \mho\Theta_2\right\| &\le \frac{1-\alpha}{\mathbb{AB}(\alpha)}\mathfrak{p}\mathbf{t}^{\mathfrak{p}-1}\mathbb{L}_{\Theta}\left\|\Theta_1 - \Theta_2\right\|_{\infty}\\ &\quad+\frac{\alpha\mathfrak{p}}{\mathbb{AB}(\alpha)\Gamma(\alpha)}\mathbb{L}_{\Theta}\left\|\Theta_1 - \Theta_2\right\|_{\infty}\int_0^{\mathbf{t}}(\mathbf{t}-\mathbf{s})^{\alpha-1}\mathbf{s}^{\mathfrak{p}-1}d\mathbf{s}\\ &\le \frac{1-\alpha}{\mathbb{AB}(\alpha)}\mathfrak{p}\mathbf{t}^{\mathfrak{p}-1}\mathbb{L}_{\Theta}\left\|\Theta_1 - \Theta_2\right\|_{\infty}\\ &\quad+\frac{\alpha\mathfrak{p}}{\mathbb{AB}(\alpha)\Gamma(\alpha)}\mathbb{L}_{\Theta}\left\|\Theta_1 - \Theta_2\right\|_{\infty}\mathbf{t}^{\alpha+\mathfrak{p}-3}B_1(\mathfrak{p},\alpha). \end{aligned}$$

Thus,

$$\begin{aligned} \left\|\mho\Theta_1 - \mho\Theta_2\right\| &\le \left(\frac{1-\alpha}{\mathbb{AB}(\alpha)}\mathfrak{p}\mathbf{t}^{\mathfrak{p}-1}\mathbb{L}_{\Theta} + \frac{\alpha\mathfrak{p}}{\mathbb{AB}(\alpha)\Gamma(\alpha)}\mathbb{L}_{\Theta}\mathbf{t}^{\alpha+\mathfrak{p}-3}B_1(\mathfrak{p},\alpha)\right)\left\|\Theta_1 - \Theta_2\right\|_{\infty}\\ &< \left(\frac{1-\alpha}{\mathbb{AB}(\alpha)}\mathfrak{p}\mathbf{a}^{\mathfrak{p}-1}\mathbb{L}_{\Theta} + \frac{\alpha\mathfrak{p}}{\mathbb{AB}(\alpha)\Gamma(\alpha)}\mathbb{L}_{\Theta}\mathbf{a}^{\alpha+\mathfrak{p}-3}B_1(\mathfrak{p},\alpha)\right)\left\|\Theta_1 - \Theta_2\right\|_{\infty}. \end{aligned}$$

Thus, if the underlying assumption is true,

$$\mathbb{L}_{\Theta} < \frac{1-\alpha}{\mathbb{AB}(\alpha)}\mathfrak{p}\mathbf{a}^{\mathfrak{p}-1}\mathbb{L}_{\Theta} + \frac{\alpha\mathfrak{p}}{\mathbb{AB}(\alpha)\Gamma(\alpha)}\mathbb{L}_{\Theta}\mathbf{a}^{\alpha+\mathfrak{p}-3}B_1(\mathfrak{p},\alpha),$$

then the contraction condition is established, that is

$$\left\|\mho\Theta_1 - \mho\Theta_2\right\| \le \left\|\Theta_1 - \Theta_2\right\|_{\infty}.$$

As a result, proving that there is only one solution, thereby completing the proof.

Numerical configuration of fractional human liver model

The numerical scheme for the suggested human liver framework is described in this part.

Modified Adams–Bashforth method

Initially, we analyze the fractional model (11) utilizing the modified fractional Adams–Bashforth technique proposed by [40].

We apply a modified Adams–Bashforth approach to describe the essential processes in the formulation mechanism of the fractional human liver model (11) concisely. Now, we have the respective integral equation after applying the ABC integral to model (7):

$$\Omega(\mathbf{t}) - \Omega(0) = \frac{1-\alpha}{\mathbb{AB}(\alpha)}\Lambda(\mathbf{t},\Omega(\mathbf{t})) + \frac{\alpha}{\mathbb{AB}(\alpha)\Gamma(\alpha)}\int_0^{\mathbf{t}}(\mathbf{t}-\tau)^{\alpha-1}\Lambda(\tau,\Omega(\tau))d\tau.$$

Moreover, substituting $\mathbf{t} = \mathbf{t}_{\mathbf{q}+1}$, where $\mathbf{q} = 0, 1, 2, \ldots$, gives

$$\begin{aligned} \Omega(\mathbf{t}_{\mathbf{q}+1}) - \Omega(0) &= \frac{1-\alpha}{\mathbb{AB}(\alpha)}\Lambda(\mathbf{t}_{\mathbf{q}},\Omega(\mathbf{t}_{\mathbf{q}})) + \frac{\alpha}{\mathbb{AB}(\alpha)\Gamma(\alpha)}\\ &\quad\times\int_0^{\mathbf{t}_{\mathbf{q}+1}}(\mathbf{t}_{m_{1+\alpha}}-\tau)^{\alpha-1}\Lambda(\tau,\Omega(\tau))d\tau \end{aligned}$$

Table 1
Table of specified variables used in computations in human liver model.

Parameters	Explanation	Value	References
$\mathcal{U}(\mathbf{t})$	The rate of BSP in blood in time $\mathbf{t}$	$\mathcal{U}(0)=\mathbb{I}$	[34,35,39]
$\mathcal{V}(\mathbf{t})$	The rate of BSP in liver in time $\mathbf{t}$	$\mathcal{V}(0)=0$	[34,35,39]
$\mathcal{W}(\mathbf{t})$	The rate of BSP in bile in time $\mathbf{t}$	$\mathcal{W}(0)=0$	[34,35,39]
$\bar{A}$	The amount of exchange of BSP from blood to liver	0.054736	[34,35]
$\bar{B}$	The rate at which BSP is reflux from liver in blood	0.0152704	[34,35]
$\bar{C}$	The amount of exchange of BSP from liver to bile	0.0093906	[34,35].

$$= \frac{1-\alpha}{\mathbb{AB}(\alpha)}\Lambda(\mathbf{t_q},\Omega(\mathbf{t_q})) + \frac{\alpha}{\mathbb{AB}(\alpha)\Gamma(\alpha)} \times \sum_{j=0}^{\mathbf{q}}\int_{\mathbf{t}_j}^{\mathbf{t}_{j+1}}(\mathbf{t}_{m_{1+1}}-\tau)^{\alpha-1}\Lambda(\tau,\Omega(\tau))d\tau. \tag{35}$$

Taking into the consideration of the interpolation polynomial scheme, we estimate the mapping $\Lambda(\tau,\Omega(\tau))$ on $[\mathbf{t}_j,\mathbf{t}_{j+1}]$:

$$\Lambda(\tau,\Omega(\tau)) \cong \mathcal{P}_j(\tau) = \frac{\tau-\mathbf{t}_{j-1}}{\hbar}\Lambda(\mathbf{t}_j,\Omega(\mathbf{t}_j)) - \frac{\tau-\mathbf{t}_j}{\hbar}\Lambda(\mathbf{t}_{j-1},\Omega(\mathbf{t}_{j-1})).$$

(35) reduces to

$$\Omega(\mathbf{t_{q+1}}) = \Omega(0) + \frac{1-\alpha}{\mathbb{AB}(\alpha)}\Lambda(\mathbf{t_q},\Omega(\mathbf{t_q})) + \frac{\alpha}{\mathbb{AB}(\alpha)\Gamma(\alpha)}\sum_{j=0}^{\mathbf{q}}\left(\frac{\Lambda(\mathbf{t}_j,\Omega(\mathbf{t}_j))}{\hbar}\int_{\mathbf{t}_j}^{\mathbf{t}_{j+1}}(\tau-\mathbf{t}_{j-1})(\mathbf{t_{q+1}}-\tau)^{\alpha-1}d\tau - \frac{\Lambda(\mathbf{t}_{j-1},\Omega(\mathbf{t}_{j-1}))}{\hbar}\int_{\mathbf{t}_j}^{\mathbf{t}_{j+1}}(\tau-\mathbf{t}_j)(\mathbf{t_{q+1}}-\tau)^{\alpha-1}d\tau\right). \tag{36}$$

Consequently, combining the integrals included in (36), we arrived at the respective estimated result:

$$\begin{aligned}\Omega(\mathbf{t_{q+1}}) &= \Omega(0) + \frac{1-\alpha}{\mathbb{AB}(\alpha)}\Lambda(\mathbf{t_q},\Omega(\mathbf{t_q})) \\ &+ \frac{\alpha}{\mathbb{AB}(\alpha)}\sum_{j=0}^{\mathbf{q}}\left(\frac{\hbar^\alpha\Lambda(\mathbf{t}_j,\Omega(\mathbf{t}_j))}{\Gamma(\alpha+2)}\Big((\mathbf{q}+\alpha-\jmath+2) \times(\mathbf{q}-\jmath+1)^\alpha-(\mathbf{q}-\jmath)^\alpha(\mathbf{q}-\jmath+2(1+\alpha))\Big) \right. \\ &\left. - \frac{\hbar^\alpha\Lambda(\mathbf{t}_{j-1},\Omega(\mathbf{t}_{j-1}))}{\Gamma(\alpha+2)}\Big((\mathbf{q}-\jmath+1)^{\alpha+1}-(\mathbf{q}\alpha-\jmath+1+\alpha)(\mathbf{q}-\jmath)^\alpha\Big)\right).\end{aligned}$$

Newton polynomial approach

We prepare a comprehensive examination of the numerical model, which is predicated on an effective method generated by the Newton polynomial approach. This strategy, which was previously proposed in [41], is more highly efficacious than the other techniques accessible in the research. We use the equation to move forward with the strategy.

$${}^{FF}\mathbf{D}_{\mathbf{t}}^{\alpha,\mathfrak{p}}\Theta(\mathbf{t}) = \Xi(\mathbf{t},\Theta(\mathbf{t})). \tag{37}$$

Integrating the above expression, gives

$$\Theta(\mathbf{t})-\Theta(0) = \frac{1-\alpha}{\mathbb{AB}(\alpha)}\mathfrak{p}\mathbf{t}^{\mathfrak{p}-1}\Xi(\mathbf{t},\Theta(\mathbf{t})) + \frac{\alpha\mathfrak{p}}{\mathbb{AB}(\alpha)\Gamma(\alpha)}\int_0^{\mathbf{t}}(\mathbf{t}-\mathbf{s})^{\alpha-1}\mathbf{s}^{\mathfrak{p}-1}\Xi(\mathbf{t},\Theta(\mathbf{t}))d\mathbf{s}. \tag{38}$$

Setting $\mathcal{Q}(\mathbf{t},\Theta(\mathbf{t})) = \mathfrak{p}\mathbf{t}^{\mathfrak{p}-1}\Xi(\mathbf{t},\Theta(\mathbf{t}))$, then (38) reduces to

$$\Theta(\mathbf{t})-\Theta(0) = \frac{1-\alpha}{\mathbb{AB}(\alpha)}\mathcal{Q}(\mathbf{t},\Theta(\mathbf{t})) + \frac{\alpha}{\mathbb{AB}(\alpha)\Gamma(\alpha)}\int_0^{\mathbf{t}}(\mathbf{t}-\mathbf{s})^{\alpha-1}\mathcal{Q}(\mathbf{s},\Theta(\mathbf{s}))d\mathbf{s}. \tag{39}$$

At $\mathbf{t_{r+1}} = (n+1)\Delta\mathbf{t}$, we have

$$\Theta(\mathbf{t_{r+1}})-\Theta(0) = \frac{1-\alpha}{\mathbb{AB}(\alpha)}\mathcal{Q}(\mathbf{t_r},\Theta(\mathbf{t_r})) + \frac{\alpha}{\mathbb{AB}(\alpha)\Gamma(\alpha)}\int_0^{\mathbf{t_{r+1}}}(\mathbf{t_{r+1}}-\mathbf{s})^{\alpha-1}\mathcal{Q}(\mathbf{s},\Theta(\mathbf{s}))d\mathbf{s}. \tag{40}$$

Moreover, we have

$$\Theta(\mathbf{t_{r+1}}) = \Theta(0) + \frac{1-\alpha}{\mathbb{AB}(\alpha)}\mathcal{Q}(\mathbf{t_r},\Theta(\mathbf{t_r})) + \frac{\alpha}{\mathbb{AB}(\alpha)\Gamma(\alpha)}\sum_{i=2}^{\mathbf{r}}\int_{\mathbf{t}_i}^{\mathbf{t}_{i+1}}(\mathbf{t_{r+1}}-\mathbf{s})^{\alpha-1}\mathcal{Q}(\mathbf{s},\Theta(\mathbf{s}))d\mathbf{s}. \tag{41}$$

Using the Newton polynomial to approximate the mapping $\mathcal{Q}(\mathbf{t},\Theta(\mathbf{t}))$, we have

$$\begin{aligned}\mathcal{P}_{\mathbf{r}}(\mathbf{s}) = \mathcal{Q}(\mathbf{t_{r-2}},\Theta(\mathbf{t_{r-2}})) &+ \frac{\mathcal{Q}(\mathbf{t_{r-1}},\Theta(\mathbf{t_{r-1}}))-\mathcal{Q}(\mathbf{t_{r-2}},\Theta(\mathbf{t_{r-2}}))}{\Delta\mathbf{t}}(\mathbf{s}-\mathbf{t_{r-2}}) \\ &+ \frac{\mathcal{Q}(\mathbf{t_r},\Theta(\mathbf{t_r}))-2\mathcal{Q}(\mathbf{t_{r-1}},\Theta(\mathbf{t_{r-1}}))+\mathcal{Q}(\mathbf{t_{r-2}},\Theta(\mathbf{t_{r-2}}))}{2(\Delta\mathbf{t})^2} \\ &\times(\mathbf{s}-\mathbf{t_{r-2}})(\mathbf{s}-\mathbf{t_{r-1}}).\end{aligned} \tag{42}$$

Plugging (42) into (39), produces

$$\begin{aligned}\Theta^{\mathbf{r+1}} &= \Theta^0 + \frac{1-\alpha}{\mathbb{AB}(\alpha)}\mathcal{Q}(\mathbf{t_r},\Theta(\mathbf{t_r})) \\ &+ \frac{\alpha}{\mathbb{AB}(\alpha)\Gamma(\alpha)}\sum_{i=2}^{\mathbf{r}}\int_{\mathbf{t}_i}^{\mathbf{t}_{i+1}}(\mathbf{t_{r+1}}-\mathbf{s})^{\alpha-1}\left(\mathcal{Q}(\mathbf{t}_{j-2},\Theta^{j-2})\right. \\ &+ \frac{\mathcal{Q}(\mathbf{t}_{j-1},\Theta^{j-1})-\mathcal{Q}(\mathbf{t}_{j-2},\Theta^{j-2})}{\Delta\mathbf{t}}(\mathbf{s}-\mathbf{t}_{j-2}) \\ &\left.+ \frac{\mathcal{Q}(\mathbf{t}_j,\Theta^j)-2\mathcal{Q}(\mathbf{t}_{j-1},\Theta^{j-1})+\mathcal{Q}(\mathbf{t}_{j-2},\Theta^{j-2})}{2(\Delta\mathbf{t})^2}(\mathbf{s}-\mathbf{t}_{j-2})(\mathbf{s}-\mathbf{t}_{j-1})\right)d\mathbf{s}.\end{aligned} \tag{43}$$

After simplification, we have

$$\begin{aligned}\Theta^{\mathbf{r+1}} &= \Theta^0 + \frac{1-\alpha}{\mathbb{AB}(\alpha)}\mathcal{Q}(\mathbf{t_r},\Theta(\mathbf{t_r})) \\ &+ \frac{\alpha}{\mathbb{AB}(\alpha)\Gamma(\alpha)}\sum_{i=2}^{\mathbf{r}}\left\{\int_{\mathbf{t}_i}^{\mathbf{t}_{i+1}}(\mathbf{t_{r+1}}-\mathbf{s})^{\alpha-1}\mathcal{Q}(\mathbf{t}_{j-2},\Theta^{j-2})d\mathbf{s}\right. \\ &+ \int_{\mathbf{t}_i}^{\mathbf{t}_{i+1}}(\mathbf{t_{r+1}}-\mathbf{s})^{\alpha-1}\frac{\mathcal{Q}(\mathbf{t}_{j-1},\Theta^{j-1})-\mathcal{Q}(\mathbf{t}_{j-2},\Theta^{j-2})}{\Delta\mathbf{t}}(\mathbf{s}-\mathbf{t}_{j-2})d\mathbf{s} \\ &+ \int_{\mathbf{t}_i}^{\mathbf{t}_{i+1}}(\mathbf{t_{r+1}}-\mathbf{s})^{\alpha-1}\frac{\mathcal{Q}(\mathbf{t}_j,\Theta^j)-2\mathcal{Q}(\mathbf{t}_{j-1},\Theta^{j-1})+\mathcal{Q}(\mathbf{t}_{j-2},\Theta^{j-2})}{2(\Delta\mathbf{t})^2} \\ &\left.\times(\mathbf{s}-\mathbf{t}_{j-2})(\mathbf{s}-\mathbf{t}_{j-1})d\mathbf{s}\right\}.\end{aligned} \tag{44}$$

It follows that

$$\begin{aligned}\Theta^{\mathbf{r+1}} &= \Theta^0 + \frac{1-\alpha}{\mathbb{AB}(\alpha)}\mathcal{Q}(\mathbf{t_r},\Theta(\mathbf{t_r})) \\ &+ \frac{\alpha}{\mathbb{AB}(\alpha)\Gamma(\alpha)}\sum_{i=2}^{\mathbf{r}}\mathcal{Q}(\mathbf{t}_{j-2},\Theta^{j-2})\int_{\mathbf{t}_i}^{\mathbf{t}_{i+1}}(\mathbf{t_{r+1}}-\mathbf{s})^{\alpha-1}d\mathbf{s} \\ &+ \frac{\alpha}{\mathbb{AB}(\alpha)\Gamma(\alpha)}\sum_{i=2}^{\mathbf{r}}\frac{\mathcal{Q}(\mathbf{t}_{j-1},\Theta^{j-1})-\mathcal{Q}(\mathbf{t}_{j-2},\Theta^{j-2})}{\Delta\mathbf{t}} \\ &\times\int_{\mathbf{t}_i}^{\mathbf{t}_{i+1}}(\mathbf{t_{r+1}}-\mathbf{s})^{\alpha-1}(\mathbf{s}-\mathbf{t}_{j-2})d\mathbf{s} \\ &+ \frac{\alpha}{\mathbb{AB}(\alpha)\Gamma(\alpha)}\sum_{i=2}^{\mathbf{r}}\frac{\mathcal{Q}(\mathbf{t}_j,\Theta^j)-2\mathcal{Q}(\mathbf{t}_{j-1},\Theta^{j-1})+\mathcal{Q}(\mathbf{t}_{j-2},\Theta^{j-2})}{2(\Delta\mathbf{t})^2} \\ &\times\int_{\mathbf{t}_i}^{\mathbf{t}_{i+1}}(\mathbf{t_{r+1}}-\mathbf{s})^{\alpha-1}(\mathbf{s}-\mathbf{t}_{j-2})(\mathbf{s}-\mathbf{t}_{j-1})d\mathbf{s}.\end{aligned} \tag{45}$$

Simple computations yields

$$\int_{\mathbf{t}_i}^{\mathbf{t}_{i+1}}(\mathbf{t_{r+1}}-\mathbf{s})^{\alpha-1}d\mathbf{s} = \frac{(\Delta\mathbf{t})^\alpha\left\{(\mathbf{r}-\imath+1)^\alpha-(\mathbf{r}-\imath)^\alpha\right\}}{\alpha},$$

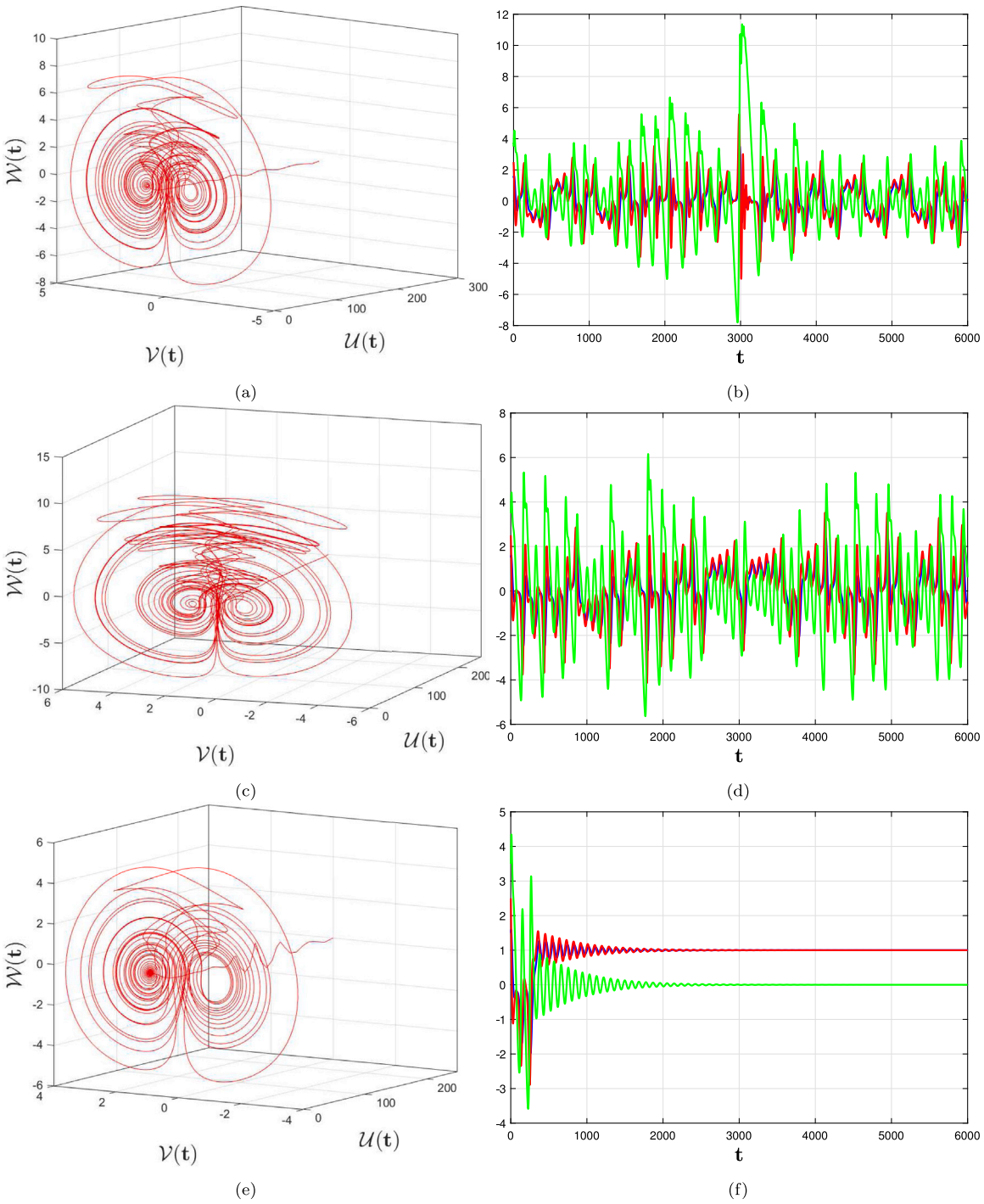

Fig. 2. Chaotic and oscillatory behavior of the fractional model (11) for various fractional orders $\alpha = 0.98,\ 0.96,\ 0.94$.

$$\int_{\mathbf{t}_\iota}^{\mathbf{t}_{\iota+1}} (\mathbf{s}-\mathbf{t}_{\iota-2})(\mathbf{t}_{\mathbf{r}+1}-\mathbf{s})^{\alpha-1} d\mathbf{s}$$
$$= \frac{(\Delta\mathbf{t})^{\alpha+1}\{(\mathbf{r}-\iota+1)^{\alpha}(\mathbf{r}-\iota+2\alpha+3)-(\mathbf{r}-\iota+1)^{\alpha}(\mathbf{r}-\iota+3\alpha+3)\}}{\alpha(\alpha+1)},$$
$$\int_{\mathbf{t}_\iota}^{\mathbf{t}_{\iota+1}} (\mathbf{t}_{\mathbf{r}+1}-\mathbf{s})^{\alpha-1}(\mathbf{s}-\mathbf{t}_{\jmath-2})(\mathbf{s}-\mathbf{t}_{\jmath-1}) d\mathbf{s} = \frac{(\Delta\mathbf{t})^{\alpha+2}}{\alpha(\alpha+1)(\alpha+2)}$$
$$\times\Big\{(\mathbf{r}-\iota+1)^{\alpha}\Big[2(\mathbf{r}-\iota)^2+(3\alpha+10)(\mathbf{r}-\iota)+2\alpha^2+9\alpha+12\Big]$$
$$-(\mathbf{r}-\iota)^{\alpha}\Big[2(\mathbf{r}-\iota)^2+(5\alpha+10)(\mathbf{r}-\iota)+6\alpha^2+18\alpha+12\Big]\Big\}. \tag{46}$$

It follows that

$$\begin{aligned}\Theta_{\mathbf{r}+1} &= \Theta_0 + \frac{1-\alpha}{\mathbb{AB}(\alpha)}\mathcal{Q}(\mathbf{t}_{\mathbf{r}},\Theta(\mathbf{t}_{\mathbf{r}}))\\ &+\frac{\alpha(\Delta\mathbf{t})^{\alpha}}{\mathbb{AB}(\alpha)\Gamma(\alpha+1)}\sum_{\iota=2}^{\mathbf{r}}\mathcal{Q}(\mathbf{t}_{\jmath-2},\Theta^{\jmath-2})\{(\mathbf{r}-\iota+1)^{\alpha}-(\mathbf{r}-\iota)^{\alpha}\}\\ &+\frac{\alpha(\Delta\mathbf{t})^{\alpha}}{\mathbb{AB}(\alpha)\Gamma(\alpha+2)}\sum_{\iota=2}^{\mathbf{r}}\Big\{\mathcal{Q}(\mathbf{t}_{\jmath-1},\Theta^{\jmath-1})-\mathcal{Q}(\mathbf{t}_{\jmath-2},\Theta^{\jmath-2})\Big\}\\ &\times\{(\mathbf{r}-\iota+1)^{\alpha}(\mathbf{r}-\iota+2\alpha+3)-(\mathbf{r}-\iota+1)^{\alpha}(\mathbf{r}-\iota+3\alpha+3)\}\end{aligned}$$

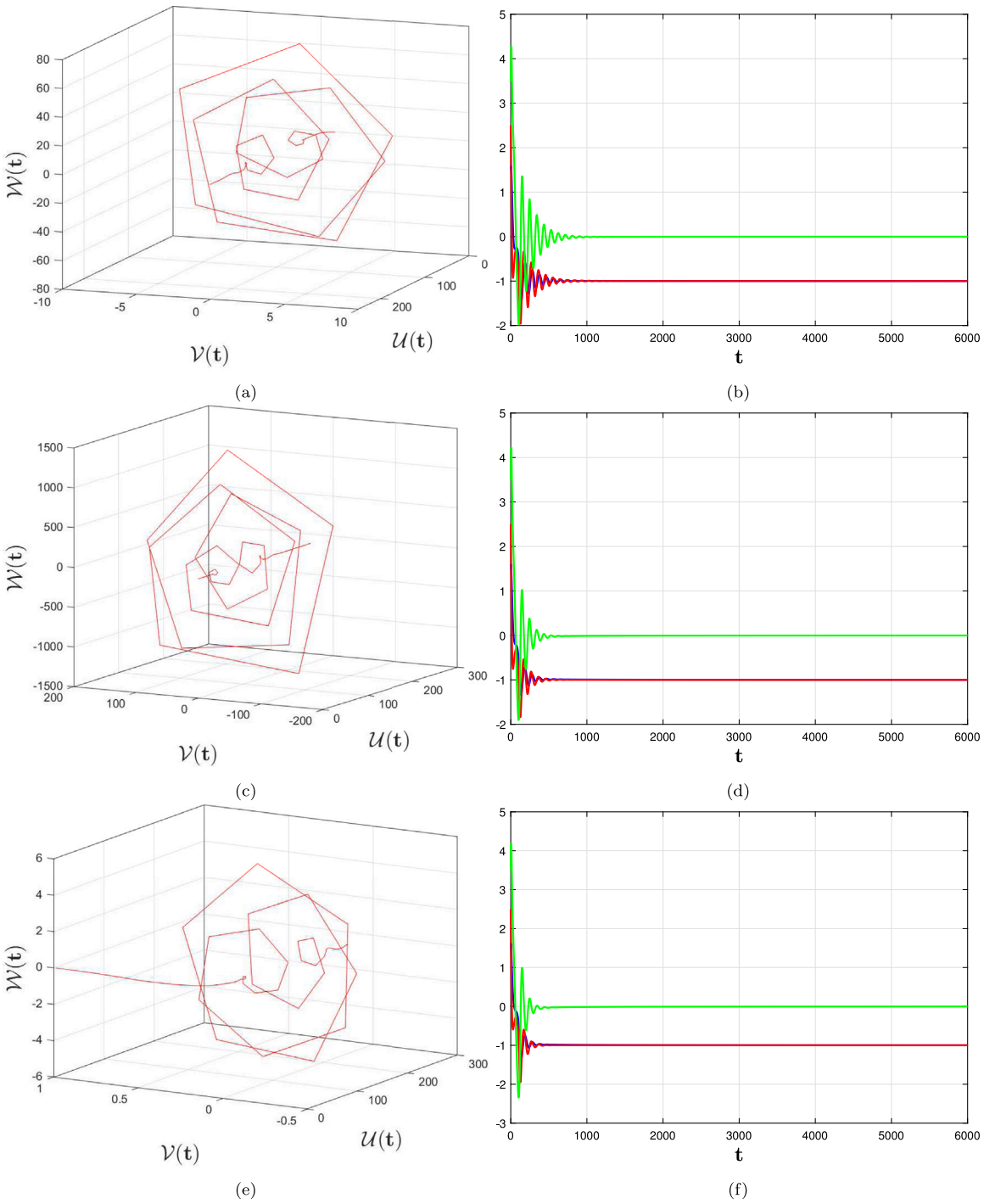

Fig. 3. Chaotic and oscillatory behavior of the fractional model (11) for various fractional orders $\alpha = 0.92,\ 0.9,\ 0.88$.

$$+\frac{\alpha(\Delta\mathbf{t})^{\alpha}}{2\mathbb{AB}(\alpha)\Gamma(\alpha+2)}\sum_{\iota=2}^{\mathbf{r}}\Big\{\mathcal{Q}(\mathbf{t}_{\jmath},\Theta^{\jmath})-2\mathcal{Q}(\mathbf{t}_{\jmath-1},\Theta^{\jmath-1})+\mathcal{Q}(\mathbf{t}_{\jmath-2},\Theta^{\jmath-2})\Big\}$$
$$\times\Big\{(\mathbf{r}-\iota+1)^{\alpha}\Big[2(\mathbf{r}-\iota)^2+(3\alpha+10)(\mathbf{r}-\iota)+2\alpha^2+9\alpha+12\Big]$$
$$-(\mathbf{r}-\iota)^{\alpha}\Big[2(\mathbf{r}-\iota)^2+(5\alpha+10)(\mathbf{r}-\iota)+6\alpha^2+18\alpha+12\Big]\Big\}. \qquad (47)$$

Hence, a generic approximate solution for human liver model:

$$\Theta_{\mathbf{r}+1}=\Theta_0+\frac{1-\alpha}{\mathbb{AB}(\alpha)}\mathfrak{p}\mathbf{t}_{\mathbf{r}}^{\mathfrak{p}-1}\mathcal{Q}(\mathbf{t}_{\mathbf{r}},\Theta(\mathbf{t}_{\mathbf{r}}))$$
$$+\frac{\alpha(\Delta\mathbf{t})^{\alpha}}{\mathbb{AB}(\alpha)\Gamma(\alpha+1)}\sum_{\iota=2}^{\mathbf{r}}\mathfrak{p}\mathbf{t}_{\iota-2}^{\mathfrak{p}-1}\mathcal{Q}(\mathbf{t}_{\jmath-2},\Theta^{\jmath-2})\{(\mathbf{r}-\iota+1)^{\alpha}-(\mathbf{r}-\iota)^{\alpha}\}$$
$$+\frac{\mathfrak{p}\alpha(\Delta\mathbf{t})^{\alpha}}{\mathbb{AB}(\alpha)\Gamma(\alpha+2)}\sum_{\iota=2}^{\mathbf{r}}\Big\{\mathbf{t}_{\iota-1}^{\mathfrak{p}-1}\mathcal{Q}(\mathbf{t}_{\jmath-1},\Theta^{\jmath-1})-\mathbf{t}_{\iota-2}^{\mathfrak{p}-1}\mathcal{Q}(\mathbf{t}_{\jmath-2},\Theta^{\jmath-2})\Big\}$$
$$\times\Big\{(\mathbf{r}-\iota+1)^{\alpha}(\mathbf{r}-\iota+2\alpha+3)-(\mathbf{r}-\iota+1)^{\alpha}(\mathbf{r}-\iota+3\alpha+3)\Big\}$$
$$+\frac{\mathfrak{p}\alpha(\Delta\mathbf{t})^{\alpha}}{2\mathbb{AB}(\alpha)\Gamma(\alpha+2)}\sum_{\iota=2}^{\mathbf{r}}\Big\{\ \mathbf{t}_{\iota}^{\mathfrak{p}-1}\mathcal{Q}(\mathbf{t}_{\jmath},\Theta^{\jmath})$$
$$-2t_{\iota-1}^{\mathfrak{p}-1}\mathcal{Q}(\mathbf{t}_{\jmath-1},\Theta^{\jmath-1})+\mathbf{t}_{\iota-2}^{\mathfrak{p}-1}\mathcal{Q}(\mathbf{t}_{\jmath-2},\Theta^{\jmath-2})\ \Big\}$$
$$\times\Big\{(\mathbf{r}-\iota+1)^{\alpha}\Big[2(\mathbf{r}-\iota)^2+(3\alpha+10)(\mathbf{r}-\iota)+2\alpha^2+9\alpha+12\Big]$$
$$-(\mathbf{r}-\iota)^{\alpha}\Big[2(\mathbf{r}-\iota)^2+(5\alpha+10)(\mathbf{r}-\iota)+6\alpha^2+18\alpha+12\Big]\Big\}. \qquad (48)$$

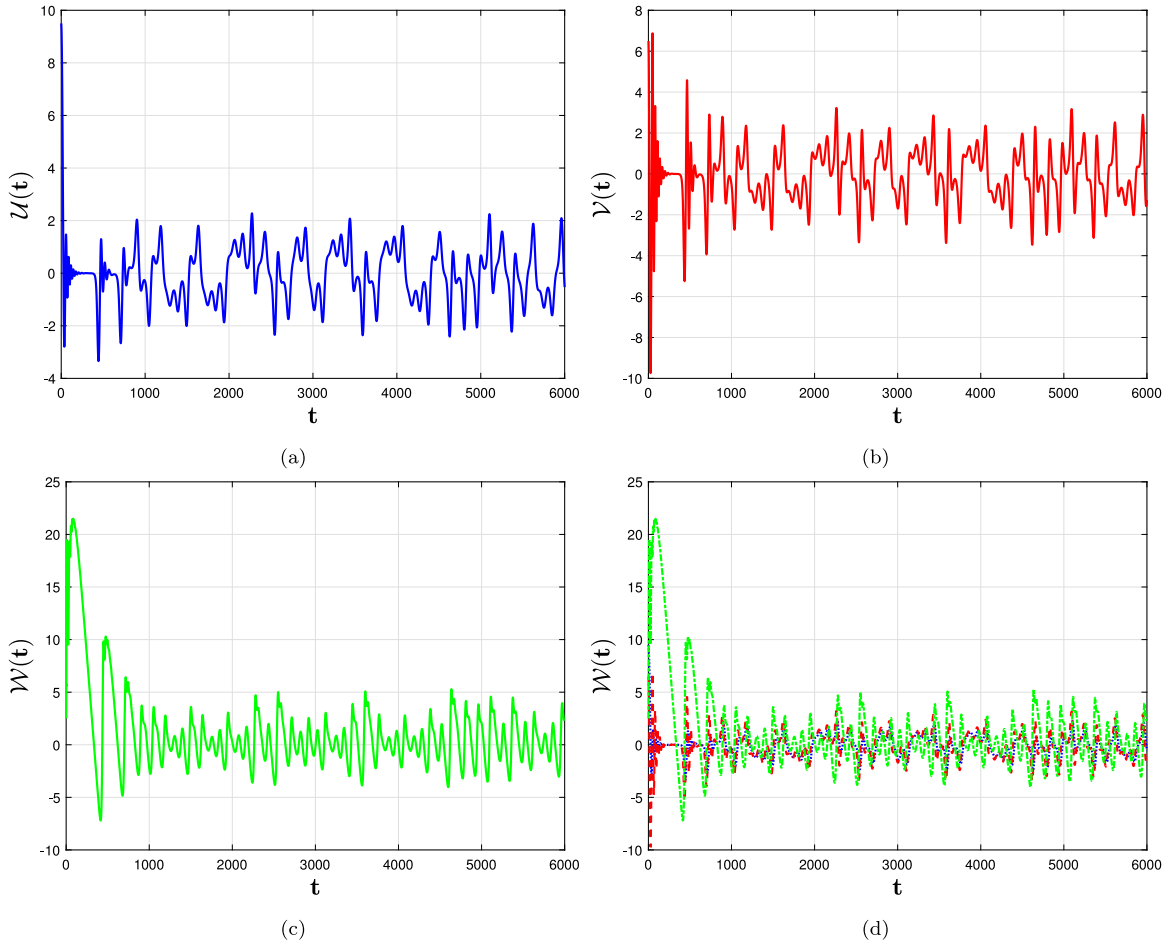

Fig. 4. Oscillatory behavior of the three compartments of fractional model (11) for fractional orders $\alpha = 0.98$.

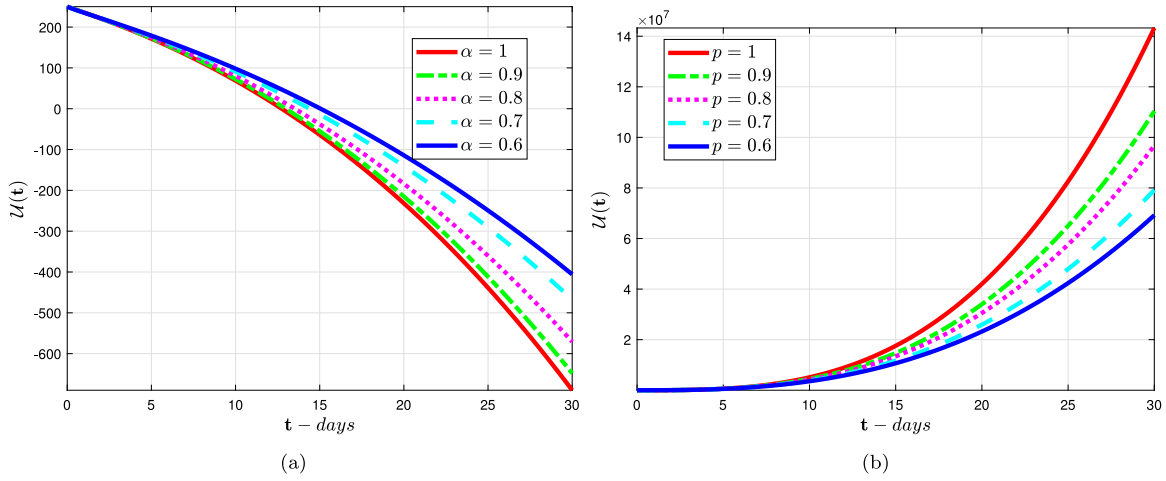

Fig. 5. (a) The effects of the human liver model (32) for the compartment $\mathcal{U}(\mathbf{t})$ of various fractional orders when fractal dimension assumed to be $\mathfrak{p} = 1$ (b) The effects of the human liver model (32) for the compartment $\mathcal{U}(\mathbf{t})$ of various fractal orders when fractional order assumed to be $\alpha = 1$.

Numerical simulation and explanation

The numerical outcomes of model (11) are now represented in the aforementioned manner. For that goal, the following basic criteria are proposed: $\mathcal{U}(0) = 250,\ \mathcal{V}(0) = 0,\ \mathcal{W}(0) = 0$ and the other parameters are shown in Table 1 as specified in [35]. The figures show any increase or decrease in the BSP blood, BSP in the liver, and BSP in bile in relation to the specific fractional order, as well as the numerical amounts of the specified variable quantities. Fig. 2(a–f) depicts the initial change in the amount of BSP in blood, which reaches a peak of roughly 20 percent of the total material contained inside the formation around the 300th minute, but then rapidly declines. Similarly, the oscillatory behavior is shown in the same context as stated above. Continuing in the same way, Fig. 3(a–f) represents the chaotic and oscillatory behavior of BSP in blood, BSP in liver and BSP in bile, respectively, for varying fractional orders by the use of ABC fractional operator sense.

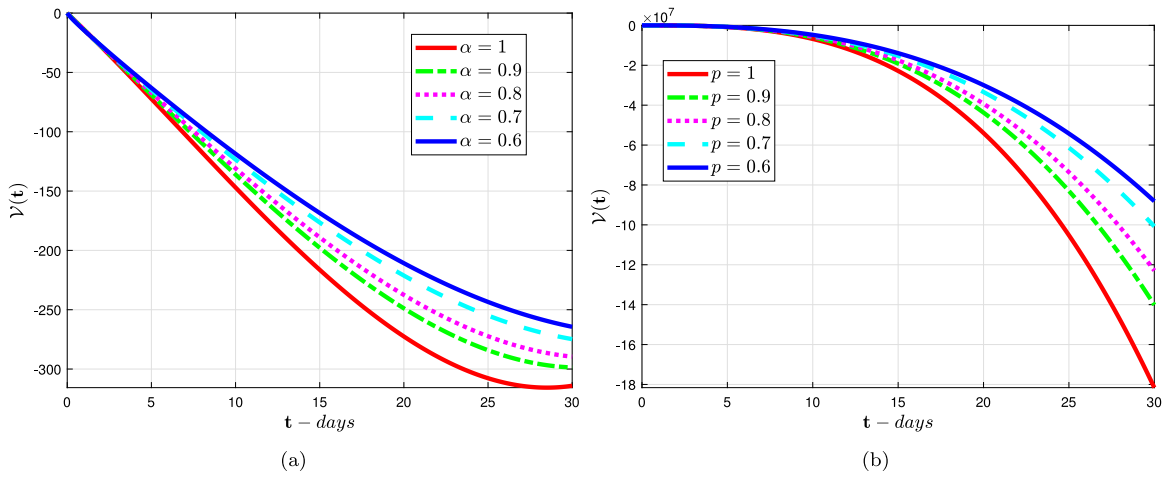

Fig. 6. The effects of the human liver model (32) for the compartment $\mathcal{V}(\mathbf{t})$ of various fractional orders when fractal dimension assumed to be $\mathfrak{p} = 1$ (b) The effects of the human liver model (32) for the compartment $\mathcal{V}(\mathbf{t})$ of various fractal orders when fractional order assumed to be $\alpha = 1$.

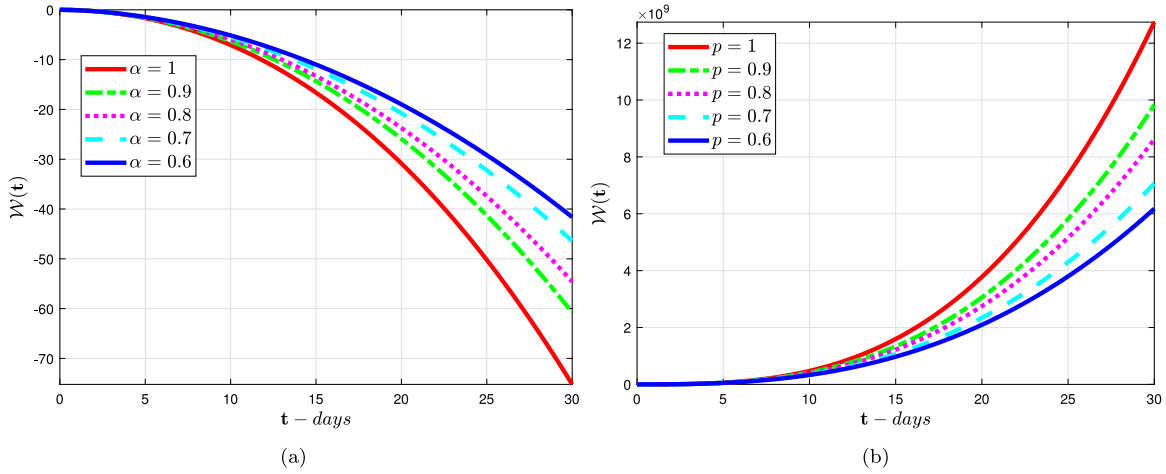

Fig. 7. The effects of the human liver model (32) for the compartment $\mathcal{W}(\mathbf{t})$ of various fractional orders when fractal dimension assumed to be $\mathfrak{p} = 1$ (b) The effects of the human liver model (32) for the compartment $\mathcal{W}(\mathbf{t})$ of various fractal orders when fractional order assumed to be $\alpha = 1$.

Table 2
Comparison analysis between clinical data (CD), generalized Mittag-Leffler function method (GMLFM), Predictor–Corrector method(PCM), Modified Adams–Bashforth method (MABM) and Newton polynomial method (NPM) for $\mathcal{U}(\mathbf{t})$.

t	0	3	5	10	20	30	43
CD [35]	250	221	184	141	98	80	64
GMLFM [33]	250	212.9644	192.2376	149.6032	101.4423	79.7121	68.0912
PCM [33]	250	212.9644	192.2376	151.3647	100.4302	79.2746	67.0912
MABM	250	212.0484	192.0000	150.2435	99.9432	78.6521	64.8760
NPM	250	211.9484	191.9260	149.9845	99.0843	77.9001	63.9865

Table 3
Comparison analysis between clinical data (CD), generalized Mittag-Leffler function method (GMLFM), Predictor–Corrector method(PCM), Modified Adams–Bashforth method (MABM) and Newton polynomial method (NPM) for $\mathcal{V}(\mathbf{t})$.

t	0	5	10	20	30
CD [35]	0	65.8	106.5	141.5	148.3
GMLFM [33]	0	56.3506	93.6406	132.6489	145.1138
PCM [33]	0	60.5824	99.2235	139.5705	148.3664
MABM	0	59.7864	98.0067	138.0834	147.6534
NPM	0	58.9340	97.9085	137.9021	146.9236

Fig. 4(a–d) depicts the oscillatory behavior of three compartments when $\alpha = 1$, it coincides with the findings predicted by [35]. The ABC fractional human liver model (11) seems to estimate many of the observations for the proportion of BSP in blood, liver, and bile, perhaps more specifically, the intermediate sets of data (diagnostic reports [35]) for every $\mathcal{U}(\mathbf{t})$, $\mathcal{V}(\mathbf{t})$ (see Fig. 4(a, b, d)), and delayed data sets $\mathcal{W}(\mathbf{t})$ (see Fig. 4 (c)–(d)). The findings are generally similar to the true experimental measurements.

Let us examine the proportion of BSP in the blood, BSP in the liver, and BSP in bile, which are three significant parameters, to demonstrate the validity of the FF fractional human liver model. Figs. 5(a–b) highlights that because of the BPS rate in blood, a larger number of nodes will be impacted relatively swiftly. To put it another way, as the fractal dimension of $\mathfrak{p} = 1$ increases, so does the blood circulation for the various fractional orders. Figs. 6(a–b) highlight as the BPS rate in liver, a larger number of nodes will be impacted relatively decreasing for various fractional order after time $\mathbf{t}$ it will becomes stable. Also, the fractal dimension $\mathfrak{p} = 1$, near to stable when fractional order is assumed to be 1. At the end, Figs. 6(a–b) represent the BPS rate in bile. A larger number of nodes will be impacted relatively swiftly. To put it another way, as the fractal dimension of $\mathfrak{p} = 1$ increases, so does the blood circulation for the various fractional orders. To test the efficacy of other possible liver brosis-blocking medicines, the majority of the evidence on anti-brotic medicines now available comes from human studies. Our system might be refined (by changing some of the characteristics) and verified when additional clinical data becomes available, and it can

Table 4
Comparison analysis between clinical data (CD), generalized Mittag-Leffler function method (GMLFM), Predictor–Corrector method(PCM), Modified Adams–Bashforth method (MABM) and Newton polynomial method (NPM) for $\mathcal{W}(\mathbf{t})$.

t	0	20	40	60	80	100	120	140	150
CD [35]	0	10.5	34.8	63.8	92.7	117	136.3	152.1	159.2
GMLFM [33]	0	9.9995	35.9872	62.9848	93.1023	113.2136	131.3963	147.1688	154.2508
PCM [33]	0	9.9993	35.9872	62.9847	93.0980	113.8444	131.8812	147.5366	154.5689
MABM	0	8.6710	34.7631	61.0067	92.1562	112.5632	130.6612	146.2398	153.2365
NPM	0	7.9900	33.0553	60.8991	91.9834	111.9670	129.0987	145.8723	152.8673

now be used to investigate the efficacy of anti-brotic therapies for the cure of liver brosis in human trials.

With $\alpha = 1$ the outcomes of the MABM, NPA, GMLFM and PCM evaluated by comparing in Tables 2–4 in full compliance with the clinical evidence, and the findings in Table 4 show that the amount of BSP in bile $\mathcal{W}(\mathbf{t})$ increases significantly. As we can see in Tables 2–4, some approximate values for MABM and NPA are similar to the real clinical examination than GMLFM and PCM. (See Fig. 7)

Conclusion

Applying a revolutionary deterministic mathematical formulation, we explored the complexities of the human liver. Basically, the system is described as a classical integer order differential problem. Furthermore, employing the generalized fractional derivative termed as the ABC operator, we expanded the liver model to fractional order in the first process. Utilizing fractional resilience ideas, the fractional human liver's local and global asymptotically stable outcomes are illustrated. Its existence and uniqueness are demonstrated using the Picard–Lindelof method. The suggested human liver model is reformulated in the second section of the research by adopting an innovative fractional-fractal operator in the AB sense. The fractional-fractal human liver model's existence and uniqueness are demonstrated. Furthermore, effective computational approaches were implemented to analyze both fractional and fractal-fractional dengue models efficiently. Lastly, several numerical models are exhibited to illustrate the relevance of the memory index and predictor variables on epidemic processes. From the visualization findings, we deduce that the fractal-fractional model delivers an excellent understanding of disease processes and can be employed as a reliable modeling framework.

Declaration of competing interest

The authors declare that they have no known competing financial interests or personal relationships that could have appeared to influence the work reported in this paper.

Acknowledgment

The authors would like to thank the reviewers and editor for their valuable comments to improve the article.

References

[1] Williams AS, Trefts E, Lantier L, Grueter CA, Bracy DP, James FD, Pozzi A, Zent R, Wasserman DH. Integrin-linked kinase is necessary for the development of diet-induced hepatic insulin resistance. Diabetes 2017;66(2):325–34.
[2] Yao Z, Li J, Guan Z, Ye Y, Chen Y. Liver disease screening based on densely connected deep neural networks. Neural Netw 2020;123:299–304.
[3] Gowda y, Desai PB, Hull VV, Math AAK, Vernekar SN, Kulkarni SS. A review on laboratory liver function tests. Pan Afr Med J 2009;3:17.
[4] Rosenthal SM, White EC. Clinical application of the bromsulphalein test for hepatic function. JAMA 1952;84(15):1112–4.
[5] Cornelius CE. Liver function. In: Clinical biochemistry of domestic animals. Elsevier; 1980, p. 201–57.
[6] Plaa G. Evaluation of hepatotoxicity: Physiological and biochemical measures of hepatic function in animals. Biology 2010. http://dx.doi.org/10.1016/B978-0-08-046884-6.01006-XCorpus, ID: 81300412.
[7] Khan MA, Khan A, Elsonbaty A, Elsadany AA. Modeling and simulation results of a fractional dengue model. Eur Phy J Plus 2019;134(8):379.
[8] Ghanbari B, Gomez-Aguilar JF. Analysis of two avian influenza epidemic models involving fractal-fractional derivatives with power and Mittag-Leffler memories. Chaos: An interdisciplinary. J Nonlinear Sci 2019;29(12):123113.
[9] Atangana A. Modelling the spread of covid-19 with new fractal-fractional operators: Can the lockdown save mankind before vaccination? Chaos Solit Fract 2020;136:109860.
[10] Sweilam NH, AL-Mekhlafi SM, Mohamed DG. Novel chaotic systems with fractional differential operators: Numerical approaches. Chaos Solit Fract 2021;142:110475.
[11] Sweilam NH, AL-Mekhlafi SM, Almutairi A. Fractal fractional optimal control for a novel malaria mathematical model; a numerical approach. Results Phy 2020;19:103446.
[12] Shen Z-H, Chu Y-M, Khan MA, Muhammad S, Al-Hartomy OA, Higazy M. Mathematical modeling and optimal control of the COVID-19 dynamics. Results Phy 2021;31:105026.
[13] Caputo M, Fabrizio M. A new definition of fractional derivative without singular kernel. Prog Fract Diff Appl 2015;1(2):73–85.
[14] Atangana A, Baleanu D. New fractional derivatives with nonlocal and non-singular kernel: theory and application to heat transfer model. Therm Sci 2016;20(00):763–9.
[15] Podlubny I. Fractional differential equations: an introduction to fractional derivatives, fractional differential equations, to methods of their solution and some of their applications. Elsevier; 1998.
[16] Jan R, Khan MA, Kumam P, Thounthong P. Modeling the transmission of dengue infection through fractional derivatives. Chaos Solit Fract 2019;127:189–216.
[17] Khan MA, Khan A, Elsonbaty A, Elsadany AA. Modeling and simulation results of a fractional dengue model. Eur Phys J Plus 2019;134(8):379.
[18] Khan MA, Ullah S, Farooq M. A new fractional model for tuberculosis with relapse via atangana– Baleanu derivative. Chaos Solit Fract 2018;116:227–38.
[19] Li X-P, Gul N, Khan MA, Bilal R, Ali A, Alshahrani MY, et al. A new Hepatitis B model in light of asymptomatic carriers and vaccination study through Atangana-Baleanu derivative. Results Phys 2021;29:104603.
[20] Li X-P, Wang Y, Khan MA, Alshahrani MY, Muhammad T. A dynamical study of SARS-COV-2: A study of third wave. Results Phys 2021;29:104705.
[21] Rashid S, Sultana S, Karaca Y, Khalid A, Chu Y-M. Some further extensions considering discrete proportional fractional operators. Fractals 2022;30(1):2240026.
[22] Cuahutenango-Barro B, Taneco-Hern1'Andez MA, Gómez-Aguilar JF. On the solutions of fractional-time wave equation with memory effect involving operators with regular kernel. Chaos Solit Fract 2018;115:283–99.
[23] Rashid S, Jarad F, Noor MA, Kalsoom H, Chu Y-M. Inequalities by means of generalized proportional fractional integral operators with respect to another function. Mathematics 2019;7(12):1225.
[24] Abdeljawad T. On conformable fractional calculus. J Comput Appl Math 2017;279:57–66.
[25] Abdeljawad T, Baleanu D. Monotonicity results for fractional difference operators with discrete exponential kernels. Adv Differential Equations 2017;2017:78.
[26] Góomez F, Rosales J, Guía M. RLC electrical circuit of non-integer order. Open Phy 2013;11(10):1361–5.
[27] Singh J, Kumar D, Kumar S. An efficient computational method for local fractional transport equation occurring in fractal porous media. Comput Appl Math 2020;39:137.
[28] Veeresha P, Prakasha DG, Singh J, Kumar D, Baleanu D. Fractional Klein–Gordon-Schrödinger equations with Mittag-Leffler memory. Chin J Phys 2020;68:65–78.
[29] Baleanu D, Jajarmi A, Sajjadi SS, Mozyrska D. A new fractional model and optimal control of a tumor-immune surveillance with nonsingular derivative operator. Chaos 2019;29:083127.
[30] Atangana A. Fractal-fractional differentiation and integration: Connecting fractal calculus and fractional calculus to predict complex system. Chaos Solit Fract 2017;102:396–406.
[31] Wang W, Khan MA. Analysis and numerical simulation of fractional model of bank data with fractal-fractional Atangana-Baleanu derivative. J Comput Appl Math 2019;369(1):112646.
[32] Li Z, Liu Z, Khan MA. Fractional investigation of bank data with fractal-fractional caputo derivative. Chaos Solit Fract 2019;131:109528.

[33] Ameen IG, Sweilam NH, Ali HM. A fractional-order model of human liver: Analytic-approximate and numerical solutions comparing with clinical data. Alexandria Eng J 2021;60:4797–808.
[34] Baleanu D, Jajarmi A, Mohammad H, Rezapour S. A new study on the mathematical modelling of human liver with Caputo–Fabrizio fractional derivative. Chaos Solit Fract 2020;134:109705.
[35] Celechovska L. A simple mathematical model of the human liver. Appl Math -Czech 2004;49(3):227–46.
[36] Ingalls BP. Mathematical modeling in systems biology: an introduction. Cambridge, MA, USA: MIT Press; 2013.
[37] Odibat ZM, Shawagfeh NT. Generalized Taylor's formula. Appl Math Comput 2007;186(1):286–93.
[38] Baleanu D, Fernandez A. On some new properties of fractional derivatives with Mittag-Leffler kernel. Commun Nonlinear Sci Numer Simul 2018;59:444–62.
[39] Arafa AAM, Hanafy IM, Gouda MI. Numerical simulations of bromsulphthalein test for human liver. Math Sci Lett 2014;3(2):75–9.
[40] Toufik M, Atangana A. New numerical approximation of fractional derivative with non-local and nonsingular kernel: application to chaotic models. Eur Phy J Plus 2017;132(10):444.
[41] Atangana A, Araz SI. New numerical scheme with newton polynomial. 1st Ed.. Elsevier; 2021.